



CERN-EP-2024-055
23 February 2024

Measurement of beauty-quark production in pp collisions at $\sqrt{s} = 13$ TeV via non-prompt D mesons

ALICE Collaboration*

Abstract

The p_T -differential production cross sections of non-prompt D^0 , D^+ , and D_s^+ mesons originating from beauty-hadron decays are measured in proton–proton collisions at a centre-of-mass energy $\sqrt{s} = 13$ TeV. The measurements are performed at midrapidity, $|y| < 0.5$, with the data sample collected by ALICE from 2016 to 2018. The results are in agreement with predictions from several perturbative QCD calculations. The fragmentation fraction of beauty quarks to strange mesons divided by the one to non-strange mesons, $f_s/(f_u + f_d)$, is found to be 0.114 ± 0.016 (stat.) ± 0.006 (syst.) ± 0.003 (BR) ± 0.003 (extrap.). This value is compatible with previous measurements at lower centre-of-mass energies and in different collision systems in agreement with the assumption of universality of fragmentation functions. In addition, the dependence of the non-prompt D meson production on the centre-of-mass energy is investigated by comparing the results obtained at $\sqrt{s} = 5.02$ and 13 TeV, showing a hardening of the non-prompt D-meson p_T -differential production cross section at higher \sqrt{s} . Finally, the $b\bar{b}$ production cross section per unit of rapidity at midrapidity is calculated from the non-prompt D^0 , D^+ , D_s^+ , and Λ_c^+ hadron measurements, obtaining $d\sigma/dy = 75.2 \pm 3.2$ (stat.) ± 5.2 (syst.) $^{+12.3}_{-3.2}$ (extrap.) μb .

arXiv:2402.16417v2 [hep-ex] 28 Oct 2024

*See Appendix A for the list of collaboration members

1 Introduction

Measuring the production of hadrons containing heavy-flavour quarks (i.e. charm and beauty) in proton–proton, pp, collisions is essential to test perturbative Quantum Chromodynamics (pQCD) calculations and provide a reference for analogous measurements in heavy-ion collisions [1]. The ALICE [2–14], ATLAS [15–17], CMS [18–22], and LHCb [23–28] experiments at the LHC have measured the production of charm and beauty hadrons and their decay leptons in pp collisions at various centre-of-mass energies (\sqrt{s}) ranging from 2.76 to 13 TeV, while RHIC [29–32], Sp \bar{p} S [33], and the Tevatron [34–37] performed measurements at lower \sqrt{s} values. The theoretical calculations rely on the factorisation of soft and hard processes [38] to predict the production cross sections of charm and beauty hadrons as a function of the transverse momentum (p_T) and the rapidity (y). According to the collinear factorisation approach, the p_T - and y -differential cross sections can be computed as the convolution of three ingredients: (i) the parton distribution functions (PDFs) describing the probability of the parton to inherit a certain fraction (x) of the momentum of the colliding proton; (ii) the partonic scattering cross section defining the scattering probability calculated as a perturbative series expansion in the strong coupling constant (α_s); (iii) the fragmentation function (FF) that describes the non-perturbative transition of a heavy-flavour quark into a hadron. The FF is parametrised from measurements performed in e^+e^- or e^-p collisions [39, 40], thus assuming the hadronisation process of charm and beauty quarks to be independent of the collision system.

Calculations for LHC energies implementing the collinear factorisation approach, like the General-Mass Variable-Flavour-Number Scheme (GM-VFNS) [41–46] and Fixed Order plus Next-to-Leading Logarithms (FONLL) [47, 48], provide a Next-to-Leading Order (NLO) accuracy with all-order resummation of next-to-leading logarithms. In addition, calculations with Next-to-Next-to-Leading-Order (NNLO) QCD radiative corrections are available for beauty-quark production. GM-VFNS and FONLL calculations describe within uncertainties the production of D mesons originating from charm-quark hadronisation (i.e. prompt) and from beauty-hadron decays (i.e. non-prompt) as a function of p_T at different centre-of-mass energies, as well as the measured production cross sections of heavy-flavour decay leptons and non-prompt J/ψ mesons originating from beauty-hadron decays [2, 7, 11, 16, 24, 25, 49–54]. Recent D and B meson measurements in small collision systems from the LHCb Collaboration [55, 56] indicate a larger production of strange over non-strange mesons when moving to a small to larger number of tracks produced in the collision. These results are strongly underestimated by predictions based on e^+e^- measurements and suggest the presence of unexpected nuclear effects also in small systems. For charm and beauty baryons, however, the pQCD calculations using FF from e^+e^- collisions severely underestimate the measured cross sections [57–63]. For instance, the prompt Λ_c^+ -baryon production cross section at low p_T and midrapidity ($|y| < 0.5$) in pp collisions at $\sqrt{s} = 5.02$ TeV [58–60, 64] is underestimated by a factor of 3 to 4 by GM-VFNS calculations adopting Λ_c^+ -baryon fragmentation functions derived from the fit of OPAL data [65], and by a factor of 15 by the POWHEG predictions [66] matched with PYTHIA 6 [67] to generate the parton shower. This discrepancy challenges the assumption of universality of the hadronisation process, i.e. the hypothesis that the parton fragmentation is independent of the collision system and energy, and can be determined from measurements in e^+e^- collisions. It is therefore crucial to extend the study of fragmentation fractions to different collision systems, centre-of-mass energies, and y intervals.

This paper presents the p_T -differential production cross sections of non-prompt D^0 , D^+ , and D_s^+ mesons at midrapidity in pp collisions at $\sqrt{s} = 13$ TeV. Sections 2 and 3 are devoted to the description of the experimental apparatus and the analysis strategy employed in this study, respectively. The sources of systematic uncertainty affecting the measurement of the production cross section and their magnitudes are detailed in Sec. 4. Section 5 reports the non-prompt D-meson cross sections compared to pQCD predictions, the ratios of D-meson species yields at $\sqrt{s} = 13$ and 5.02 TeV, and the fragmentation fraction of beauty quarks together with the total production cross section of beauty quarks at $\sqrt{s} = 13$ TeV. This

latter result supersedes the one of Ref. [68] by using a non-prompt D^0 -meson measurement with finer granularity in p_T and by including the contributions from non-prompt D^+ and D_s^+ mesons.

2 Experimental apparatus and data sample

A detailed description of the ALICE detector and its performance can be found in Refs. [69, 70]. Heavy-flavour hadron decays are reconstructed with the detectors of the central barrel, which cover the pseudorapidity range $|\eta| < 0.9$ and are located inside a cylindrical solenoid that produces a magnetic field of $B = 0.5$ T along the beam direction. Charged-particle trajectories are reconstructed by the Inner Tracking System (ITS) and the Time Projection Chamber (TPC). The ITS detector is composed of six layers of silicon detectors, which delivers precise measurements of track parameters near the interaction point, and additionally provides a resolution on the track impact parameter in the transverse plane better than $75 \mu\text{m}$ for tracks with $p_T > 1$ GeV/ c . The TPC provides track reconstruction featuring up to 159 three-dimensional space points per track, as well as charged particle identification (PID) through specific energy loss (dE/dx) measurements. Additionally, the Time-Of-Flight (TOF) detector measures the flight time of charged particles, providing additional constraints for the identification of the decay products of heavy-flavour hadrons. Trigger and event selections are performed using the V0 detector, which comprises two scintillator arrays located on either side of the collision point and that cover the pseudorapidity ranges $-3.7 < \eta < -1.7$ and $2.8 < \eta < 5.1$.

The measurements reported in this article were performed on the data sample of pp collisions at $\sqrt{s} = 13$ TeV collected with the ALICE experiment from 2016–2018. The pp collisions were recorded using a minimum bias (MB) trigger that required coincident signals in both V0 scintillator arrays. Beam-induced background events, including beam–gas interactions and pileup of collisions from different bunch crossings, were removed offline using the timing information from the V0 arrays and correlating the number of measured clusters and tracks reconstructed in the two innermost layers of the ITS. Events with pileup of collisions within the same bunch crossing were eliminated by rejecting events with more than one reconstructed primary vertex. Moreover, to ensure uniform pseudorapidity acceptance, only events with a primary vertex position within ± 10 cm from the nominal centre of the apparatus along the beam direction were considered. The analysed data consisted of about 1.8×10^9 MB collisions, corresponding to an integrated luminosity $\mathcal{L}_{\text{int}} = 31.9 \pm 0.5 \text{ nb}^{-1}$ [71].

To correct for detector acceptance and efficiency and to train the machine learning algorithms that are used in this analysis as described later, Monte Carlo (MC) simulations of pp collisions at the same centre-of-mass energy were utilised. These MC samples were generated using the PYTHIA 8.243 [72] event generator, requiring the production of at least one $c\bar{c}$ or $b\bar{b}$ pair in each simulated event. The produced charm hadrons were forced to decay in the decay channels of interest. The generated particles were transported through the apparatus with GEANT3 [73], including a realistic description of the detector conditions during the data taking.

3 Data analysis

The D mesons and their charge conjugates were reconstructed through the following hadronic decay channels: $D^0 \rightarrow K^-\pi^+$ with $\text{BR} = (3.95 \pm 0.03)\%$, $D^+ \rightarrow K^-\pi^+\pi^+$ with $\text{BR} = (9.38 \pm 0.16)\%$, and $D_s^+ \rightarrow \phi\pi^+ \rightarrow K^+K^-\pi^+$ with $\text{BR} = (2.22 \pm 0.06)\%$ [74]. The D-meson candidates were reconstructed by combining tracks with $|\eta| < 0.8$ and $p_T > 0.3$ GeV/ c . Only tracks crossing at least 70 pad rows in the TPC, having at least one associated hit in the two innermost ITS layers, and passing the track-quality criteria described in Ref. [3] were considered. Pions and kaons were identified by requiring the dE/dx and time-of-flight signals to be compatible with the expected values within three times the detector resolution. The selections applied to the single tracks affect the D-meson reconstruction and acceptance as a function of the rapidity, which decreases steeply for $|y| > 0.5$ at $p_T < 5$ GeV/ c and $|y| > 0.8$ for

$p_T > 5$ GeV/c. For this reason, a p_T -dependent selection was applied on the D-meson rapidity to define a fiducial acceptance, $|y| < y_{\text{fid}}(p_T)$, with $y_{\text{fid}}(p_T)$ increasing from 0.5 to 0.8 in $0 < p_T < 5$ GeV/c and $y_{\text{fid}} = 0.8$ above 5 GeV/c. This is also taken into account when computing the acceptance term in the cross section formula.

A Boosted Decision Tree (BDT) algorithm was employed to reduce the sizeable combinatorial background and to improve the separation between the contributions of prompt and non-prompt D mesons through a multi-class classification approach [75]. The implementation of the BDT algorithm provided by the XGBoost [76, 77] library was employed for the results presented in this work. The machine learning algorithm was provided with signal examples of D mesons from simulations based on the PYTHIA 8.243 event generator, while the background samples were obtained from the “sideband” region of the D-meson candidate invariant-mass (M) distributions in data. For D^0 and D^+ , this region was defined as the invariant-mass intervals $|\Delta M| > 5\sigma$ with respect to the nominal value of their respective mass (i.e. $M < 1.80$ GeV/c² and $M > 1.95$ GeV/c² for D^0 and $M < 1.82$ GeV/c² and $M > 1.92$ GeV/c² for D^+). For D_s^+ mesons, the regions $M < 1.82$ GeV/c² and $M > 2.01$ GeV/c² were considered, corresponding to masses of the order of 5σ below the nominal D^+ mass and 5σ above the nominal D_s^+ mass. This selection was tuned to efficiently reject the contribution from D^+ mesons decaying in the same decay channel. Loose selection criteria were applied to the D-meson candidates before the BDT training, following the same procedures described in Refs. [3, 78, 79]. For the D_s^+ -meson candidates, an additional selection was applied on the reconstructed value of the K^+K^- invariant mass to be consistent with the Particle Data Group world average of the ϕ -meson rest mass ($M(\phi) = 1019.461 \pm 0.016$ [74]) with ± 15 MeV/c². The variables provided to the BDT algorithm to classify the candidates as either D mesons originating from beauty-hadron decays, prompt D mesons, or background candidates, include those related to the decay-vertex topology and single-track PID, which have proven to strongly influence the score assigned by the BDT. In particular, the impact of each input variable was assessed via the SHAP package [80]. The complete list of input variables can be found in Ref. [78]. The information about variables related to the decay-vertex topology was found to be the most relevant to discriminate signal and background candidates, as expected. Independent BDTs were trained for the different p_T intervals of the analyses and the resulting optimised algorithms were applied to the data, where the type of candidate is unknown. The BDT provides three different outputs, one for each class, representing the estimated probability of a candidate to be a prompt D meson, a non-prompt D meson, or combinatorial background. Selections were applied on both the probability to be a non-prompt D meson and on the probability to be combinatorial background. The first selection was meant to enhance the non-prompt contribution within the selected signal, and the second one was employed to reject the largest possible amount of combinatorial background as possible, while preserving the signal candidates. Different selection criteria on the BDT outputs were used in the analysis in order to build samples with different fractions of non-prompt (and prompt) D mesons [75, 78, 79].

The raw yields of D mesons (sum of particles and antiparticles) were measured in the range $1 < p_T < 24$ GeV/c for D^0 and D^+ mesons and $2 < p_T < 24$ GeV/c for D_s^+ mesons. The raw yields were extracted by performing a binned maximum-likelihood fit of the invariant mass distributions of candidates satisfying the BDT selection criteria. These criteria enhance the fraction of non-prompt D mesons, $f_{\text{non-prompt}}^{\text{raw}}$, in the sample, referred to as the non-prompt enhanced sample. The signal peak was parameterised with a Gaussian function, whose width was constrained to match the one extracted from fits to the prompt-enhanced sample evaluated in this work, i.e. candidates passing BDT selection criteria providing a significant fraction of prompt D mesons. For the D^0 meson, the contribution of signal candidates to the invariant-mass distribution with the wrong mass assigned to the D^0 -decay tracks (reflections) was included in the fit. It was estimated based on the invariant-mass distributions of the reflected signal in the simulation, which were described as the sum of two Gaussian functions. The contribution of reflections to the raw yield is about 0.5–1.5%, depending on p_T . This constraint improved the stability of the fits because the prompt-enhanced sample has a higher statistical significance compared

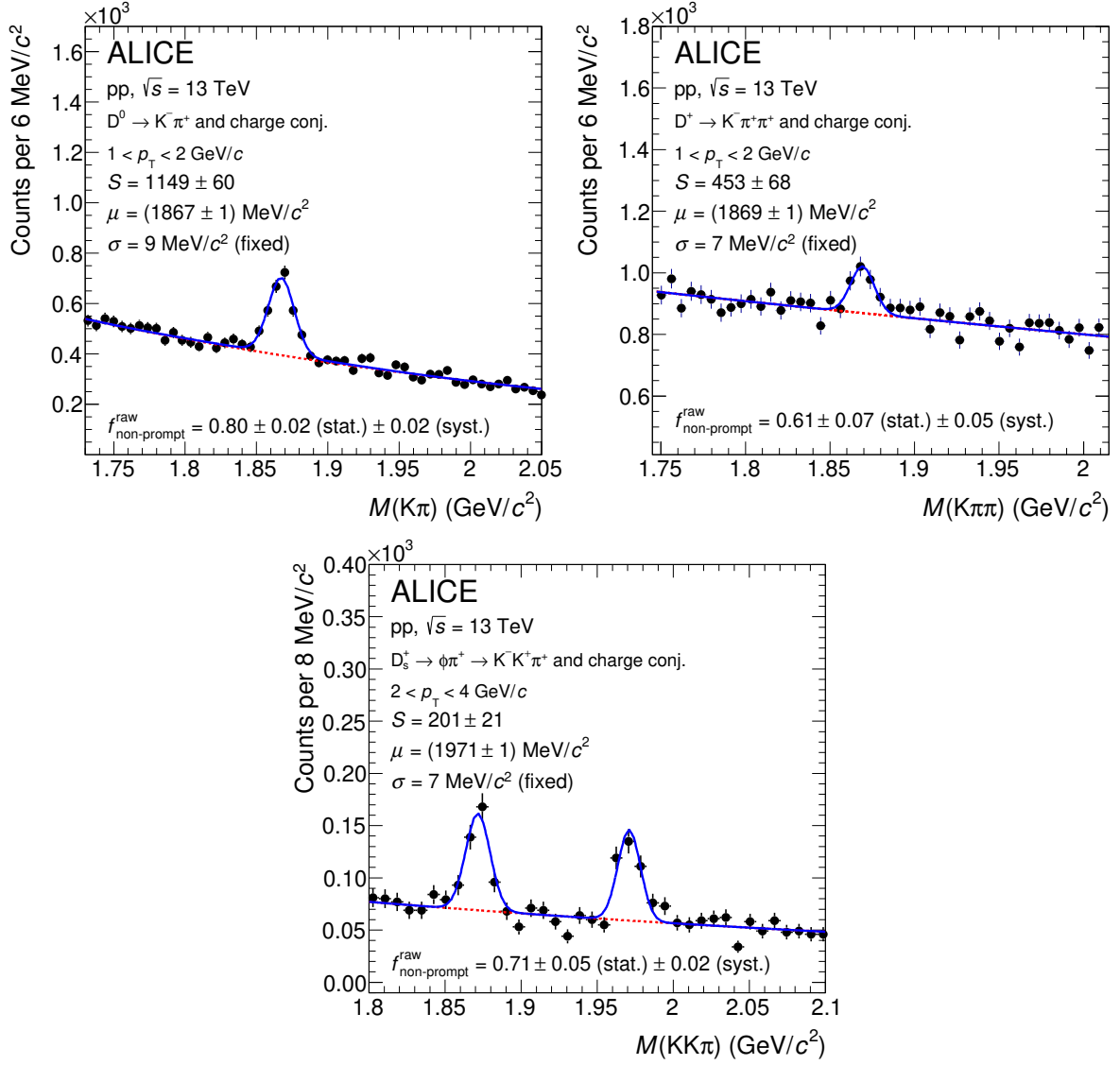


Figure 1: Invariant-mass distributions of non-prompt enhanced D^0 - (top-left), D^{+-} (top-right), and D_s^+ -meson (bottom) candidates, and their charge conjugates in $1 < p_T < 2$ GeV/c, $1 < p_T < 2$ GeV/c, and $2 < p_T < 4$ GeV/c, respectively. For the D_s^+ meson, the left-side peak emerges due to the contribution of the D^+ meson decaying in the same channel as the D_s^+ meson. The blue solid line shows the total fit function and the red dashed line the combinatorial-background contribution. The values of the mean (μ), width (σ), and raw yield (S) of the signal peak are reported together with their statistical uncertainties resulting from the fit. The width is fixed to the one obtained from the prompt-enhanced sample. The fraction of non-prompt candidates in the measured raw yield is reported with its statistical and systematic uncertainties.

to the non-prompt enhanced one due to the larger abundance of prompt D mesons compared to non-prompt D mesons. The background was modelled with an exponential function. In the fit to the invariant-mass distributions of D_s^+ -meson candidates, an independent Gaussian function was adopted to model the peak related to $D^+ \rightarrow \phi \pi^+ \rightarrow K^+ K^- \pi^+$ decays. Figure 1 shows examples of fits to the invariant-mass distributions of D^0 , D^+ , and D_s^+ candidates for the non-prompt D-meson enhanced samples in the lowest p_T interval accessible in the respective analyses.

The p_T -differential cross section of non-prompt charm hadrons at midrapidity was computed as:

$$\left. \frac{d\sigma_{\text{non-prompt}}^{\text{D}}}{dp_T} \right|_{|y| < 0.5} = \frac{1}{2} \frac{1}{\Delta p_T} \frac{f_{\text{non-prompt}}^{\text{raw}} N_{|y| < y_{\text{fid}}}^{\text{D}+\bar{\text{D}}}}{c_{\Delta y}(\text{Acc} \times \varepsilon)_{\text{non-prompt}}} \cdot \frac{1}{\text{BR}} \cdot \frac{1}{\mathcal{L}_{\text{int}}}. \quad (1)$$

The term $N_{|y| < y_{\text{fid}}}^{\text{D}+\bar{\text{D}}}$ refers to the raw yields in the various p_T intervals, extracted as described above. This quantity was then scaled by the non-prompt fraction $f_{\text{non-prompt}}^{\text{raw}}$ to account for prompt D-meson signals in the raw yield, and divided by 2 to obtain the averaged yields between particles and antiparticles. The raw yield was corrected by the $c_{\Delta y}(\text{Acc} \times \varepsilon)_{\text{non-prompt}}$ term, which accounts for the fiducial interval in rapidity ($c_{\Delta y} \simeq 2y_{\text{fid}}$), the detector acceptance, and the reconstruction and selection efficiency of the non-prompt D-meson signal. The production cross section in each p_T interval was then obtained by scaling the corrected yield of non-prompt D mesons by the p_T -interval width (Δp_T), the branching ratio of the decay channel chosen to reconstruct the signal (BR), and the integrated luminosity (\mathcal{L}_{int}).

The $c_{\Delta y}(\text{Acc} \times \varepsilon)_{\text{non-prompt}}$ and the $f_{\text{non-prompt}}^{\text{raw}}$ terms for D^0 , D^+ , and D_s^+ mesons are reported as a function of p_T in the left and right panels of Fig. 2, respectively. The $(\text{Acc} \times \varepsilon)_{\text{non-prompt}}$ is obtained as the product of the selection efficiency ε , accounting for the D mesons simulated with PYTHIA 8 surviving the selection criteria, and the geometrical acceptance of the experimental apparatus estimated with GEANT3. The $c_{\Delta y}$ term is introduced to normalise the D-meson yield to one unit of rapidity, thus accounting for the rapidity coverage of the measurements in $|y| < y_{\text{fid}}(p_T)$, and is found to be compatible with unity in PYTHIA simulations. The fraction $f_{\text{non-prompt}}^{\text{raw}}$ was estimated with a data-driven procedure based on constructing data sub-samples with different abundances of prompt and non-prompt candidates. The samples were built by gradually varying solely the selection criterion on the BDT output related to the candidate's estimated probability to be a non-prompt D meson, while keeping the criterion on the probability to be background fixed to the nominal one. An equation relates the BDT selection efficiency of prompt and non-prompt D mesons and the extracted raw yields from each BDT selection criterion to the true yields of prompt and non-prompt D mesons, forming a system of equations used to estimate the $f_{\text{non-prompt}}^{\text{raw}}$. The effectiveness of this method was demonstrated in previous similar analyses, as documented in Refs. [75, 78, 79]. Fractions of non-prompt candidates larger than 70% (60%) were obtained for D^0 (D^+ and D_s^+) mesons in all the p_T intervals of the analysis. This shows that the BDT-based selections substantially enhance the non-prompt component in the raw yields with respect to the naturally produced fractions of non-prompt mesons, which range from 5% at low p_T to 15% at high p_T .

4 Systematic uncertainties

The following sources of systematic uncertainty were considered for the non-prompt D-meson production cross sections: (i) the raw-yield extraction, (ii) track-reconstruction efficiency estimation, (iii) PID efficiency evaluation, (iv) non-prompt fraction estimation, (v) D-meson selection efficiency determination, and (vi) D-meson simulated p_T shape estimation. The sources (ii)–(vi) originate from possible differences between data and simulation due to imperfections in modelling particle interactions, the description of the detector response and alignment, or the underlying physics processes in the simulation. The resulting systematic uncertainties on the non-prompt D-meson production cross section in representative p_T intervals are summarised in Table 1. The systematic uncertainty assigned to the measured p_T -differential cross section is computed as the sum in quadrature of the uncertainties listed below.

The systematic uncertainty on the raw-yield extraction was assessed by varying the background fit function (linear and parabolic), the binning of the invariant-mass distribution, and the upper and lower fit limits. The sensitivity to the line shape of the D-meson peak was tested by comparing the raw-yield values from the fits with those obtained by counting the candidates in the invariant-mass region of the signal after subtracting the background estimated from a fit to the sidebands. For non-prompt D^0 mesons,

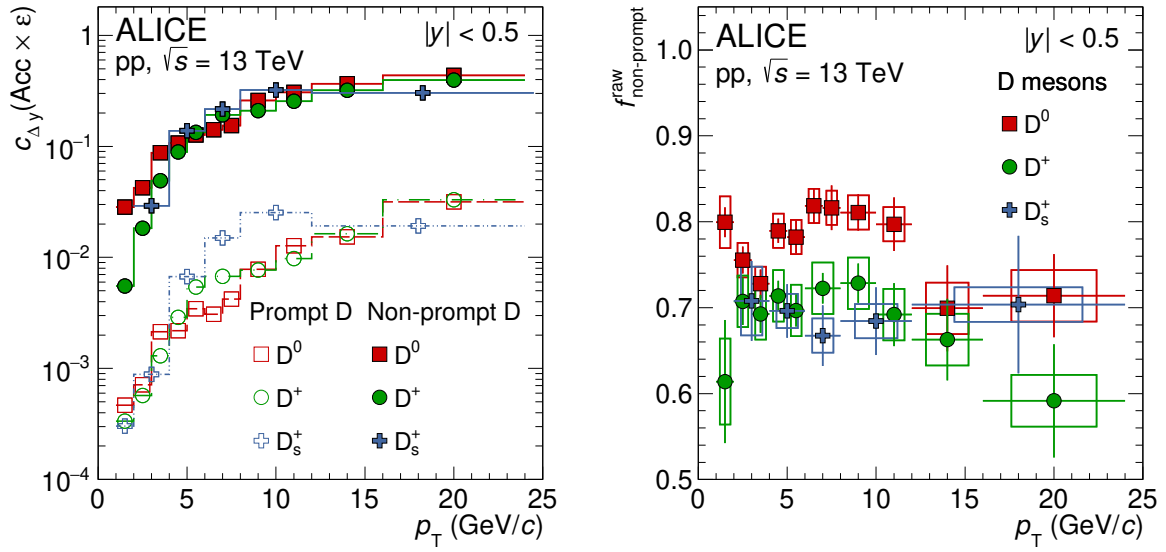


Figure 2: Left: $c_{\Delta y}(Acc \times \epsilon)$ factors of the selection criteria of the analyses for prompt and non-prompt D mesons as a function of p_T . Right: raw fraction of non-prompt D^0 , D^+ , and D_s^+ mesons in the raw yield as a function of p_T . The vertical bars and boxes display the statistical and systematic uncertainties, respectively.

an additional contribution due to the description of signal reflections in the invariant-mass distribution was estimated by varying the shape and the normalisation of the templates used for the reflections in the invariant-mass fits. The magnitude of this source of systematic uncertainty is assessed by considering the shift and the root mean square of the trial raw yield distribution with respect to the reference value and it ranges between 2% and 10% depending on the D-meson species and p_T .

The systematic uncertainty on the track-prolongation reconstruction efficiency accounts for possible discrepancies between data and MC in the TPC–ITS prolongation efficiency and the selection efficiency on track-quality criteria in the TPC. The per-track systematic uncertainties were estimated by varying the track-quality selection criteria and comparing the TPC tracks' prolongation probabilities to the ITS clusters in data and simulations. They were then propagated to the non-prompt D meson systematic uncertainty via their decay kinematics. Furthermore, a non-optimal description of the material budget in MC could cause a bias in the estimation of the selection efficiency. This discrepancy was handled by comparing the selection efficiency obtained using simulations with different material budgets. The magnitude of this source of systematic uncertainty depends on p_T , and it ranges from 4% to 6% for the two-body decays of D^0 mesons and from 5% to 8% for D^+ and D_s^+ mesons, which are reconstructed via three-particle decay channels.

A possible systematic uncertainty on the PID selection efficiency was also considered. This source was evaluated in the prompt D-meson analysis [14], and it was found to be negligible for the adopted PID strategy for all the three D meson species.

The systematic uncertainties on the estimation of the BDT-selection efficiency and the non-prompt D-meson fraction account for discrepancies between data and MC simulations in the distributions of the variables used in the BDT-model training (i.e. the D-meson decay-vertex topology, kinematics, and PID variables). The former was studied by repeating the entire analysis, varying the BDT selection criteria. The uncertainty was computed as the quadratic sum of the root mean square (RMS) and the shift in the distribution of the corrected yields derived from the variation of the BDT selection in relation to the reference value. The systematic uncertainty of the non-prompt fraction was estimated by varying the configuration of the BDT selections included in the data-driven method described in Section 3. The selections based on the BDT probabilities were varied considering looser and tighter conditions

Table 1: Relative systematic uncertainties of the measured cross sections of non-prompt D^0 , D^+ , and D_s^+ mesons at midrapidity in pp collisions at $\sqrt{s} = 13$ TeV. The values reported in the table refer to representative p_T intervals of the different channels.

p_T (GeV/c)	D^0		D^+		D_s^+	
	1–2	12–16	1–2	12–16	2–4	12–24
Signal extraction	4%	3%	5%	5%	3%	5%
Tracking efficiency	4%	5%	6%	8%	5%	8%
Non-prompt fraction	2%	2%	5%	3%	4%	2%
Selection efficiency	4%	2%	10%	4%	3%	3%
MC p_T shape	6%	1%	7%	2%	3%	2%
Branching ratio	0.8%		1.7%		2.7%	
Luminosity	1.6%					
Total uncertainty	9.5%	7.9%	15.5%	12.0%	8.7%	10.6%

on the probability of the D-meson candidates being non-prompt D mesons. The non-prompt D-meson fraction was computed for each configuration, and the systematic uncertainty was assigned considering the variation with respect to the reference case. The magnitude of these uncertainties ranges between 2 and 5% for the non-prompt D-meson fraction and from 2 to 10% for the BDT selection efficiency, depending on the D-meson species and p_T . In particular, the uncertainty due to the selection efficiency is larger at low p_T where more stringent selection criteria are applied.

The calculation of the $(\text{Acc} \times \varepsilon)$ factor can be influenced by differences between the hadron p_T distributions generated in the simulation and those in data. To estimate the uncertainty the simulated p_T distributions were weighted to match the p_T spectra derived from FONLL calculations instead of those from PYTHIA 8 simulations. In particular, the FONLL and PYTHIA 8.243 predictions for D mesons were used to compute the weights for prompt D mesons, while for non-prompt D mesons, the spectra of the beauty-hadron parents were considered. The $(\text{Acc} \times \varepsilon)$ correction factor and the raw non-prompt D meson fraction were then recomputed employing the weighted spectra, and a comparison was made between the reference and the weighted cases. The difference between these two results was assigned as a systematic uncertainty. The magnitude of this uncertainty ranges between 1 and 7% and it is larger in the low- p_T intervals where the efficiency steeply increases with p_T .

Finally, the uncertainties on the BR of the analysed decay channel of the three D-meson species (0.8% for D^0 , 1.7% for D^+ , and 2.7% for D_s^+) [74] and the integrated luminosity in pp collisions (1.6%) [71] were considered.

5 Results

5.1 Non-prompt D-meson p_T -differential cross sections

The p_T -differential production cross sections of non-prompt and prompt D^0 , D^+ , and D_s^+ mesons at midrapidity, $|y| < 0.5$, in pp collisions at a centre-of-mass energy of 13 TeV are shown in the left panel of Fig. 3. The prompt D-meson cross sections are from Ref. [14]. The vertical lines and empty boxes represent the statistical and systematic uncertainties. Note that the systematic uncertainties shown in the plots do not include contributions from luminosity and branching ratio.

The right panels of Fig. 3 display the ratios among the p_T -differential production cross sections of non-prompt and prompt D^0 (top panel), D^+ (middle panel), and D_s^+ (bottom panel) mesons at both $\sqrt{s} = 5.02$ [78] and 13 TeV. The systematic uncertainties of the ratio calculations are treated as uncorrelated among prompt and non-prompt D mesons, except for those associated with the tracking,

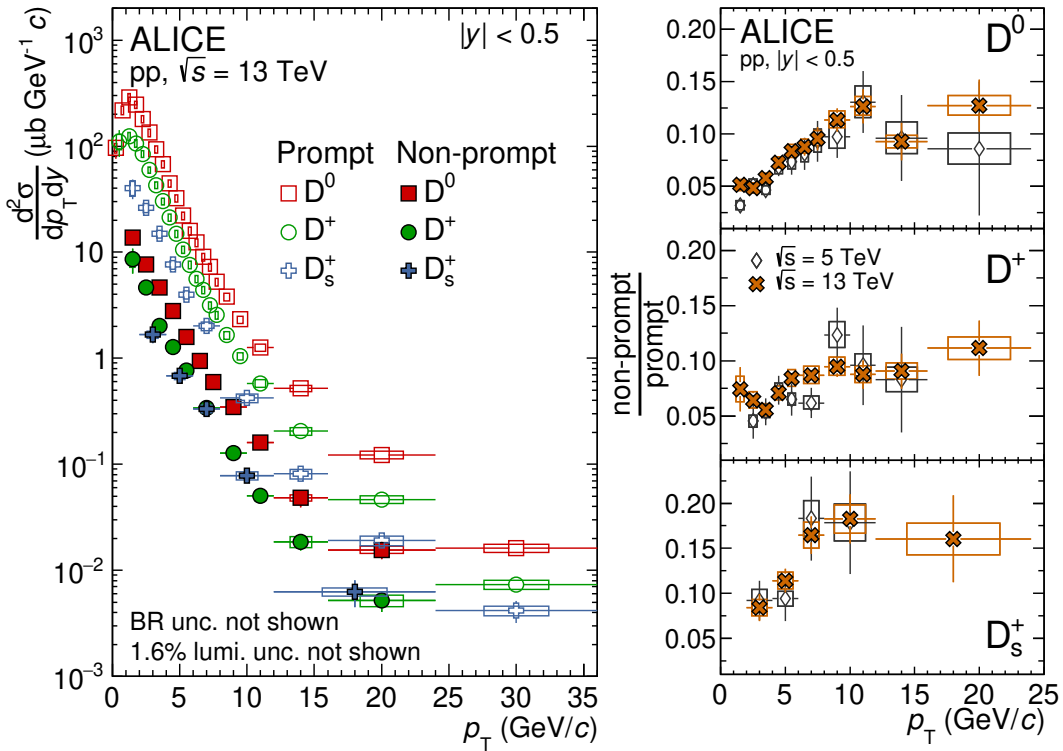


Figure 3: Left: p_T -differential production cross sections of prompt [14] and non-prompt D^0 , D^+ , and D_s^+ mesons at midrapidity, $|y| < 0.5$, in pp collisions at $\sqrt{s} = 13$ TeV. Right: ratios between the production cross sections of non-prompt and prompt D^0 (top), D^+ (middle), and D_s^+ (bottom) mesons at $\sqrt{s} = 5.02$ [78] and 13 TeV. The vertical bars and empty boxes represent the statistical and systematic uncertainties, respectively.

luminosity, and BR, which are considered as fully correlated.

The uncertainties on the luminosity and the BR cancel out in the ratio. The production of prompt D mesons exceeds that of non-prompt D mesons for all D-meson species by about a factor of 20 at low p_T . The larger abundance of prompt charm mesons is expected owing to the lower mass of charm with respect to beauty quarks. The ratios exhibit an increasing trend as a function of p_T up to approximately 12 GeV/c , consistent within uncertainties between the two centre-of-mass energies. This rise reflects the harder transverse-momentum spectrum of beauty hadrons (h_b) with respect to that of prompt charm mesons.

In Fig. 4, the p_T -differential cross sections of non-prompt D mesons are compared with the predictions obtained from FONLL [47, 48] and GM-VFNS [41, 42, 81] calculations. In these models, the fragmentation fractions of beauty quarks into different beauty-hadron species, denoted as $f(b \rightarrow B)$, are derived from e^+e^- collisions [39]. The results of calculations based on the TAMU model [82], which adopts the p_T -differential beauty-quark cross section from FONLL along with the same fragmentation functions employed in FONLL and a statistical hadronisation approach for $f(b \rightarrow B)$, are also shown in Fig. 4. In this statistical approach, chemical equilibrium among beauty-hadron species is assumed, and the relative abundances of different hadrons are determined by their masses and a universal hadronisation temperature. In the case of FONLL and TAMU predictions, the resulting beauty hadron cross section is convoluted with the decay kinematics and branching ratios of $h_b \rightarrow h_c + X$ obtained using PYTHIA 8.243 [72, 83] to compute the non-prompt D-meson cross section. In the context of GM-VFNS, the transition from the beauty quark to the observed charm-hadron state is described via a two-step approach. This involves the hadronisation of the beauty quark into the beauty hadron ($b \rightarrow h_b$) and its subsequent decay into the measured charm meson ($h_b \rightarrow D + X$). Even though an alternative decay path that

accomplishes this transition in a single step exists ($b \rightarrow D + X$), it significantly underestimates the predictions derived from the former approach and the measured cross sections, as already observed in Ref. [78]. The theoretical uncertainties associated with the FONLL and GM-VFNS predictions are shown as boxes. These uncertainties encompass variations in the factorisation scale (μ_F), renormalisation scale (μ_R), heavy-quark mass value, and the uncertainty of the CTEQ6.6 [84] and CT14nlo [85] parton distribution functions, respectively. Consistent with previous studies at lower collision energy [78], FONLL calculations describe the measured non-prompt D-meson production cross sections within uncertainties. In particular, the central values of the FONLL+PYTHIA 8 predictions are consistent with the data for the three D-meson species. The TAMU predictions using the statistical hadronisation approach for the abundances of different hadron species agree with the measured cross sections of non-prompt D^0 and D^+ mesons. However, they tend to overestimate the yield of non-prompt D_s^+ mesons. The GM-VFNS calculations underestimate the measurements in the low- p_T region, whereas at higher p_T a better agreement is found.

5.2 Cross section ratios

The p_T -differential D^+/D^0 and $D_s^+/(D^0 + D^+)$ yield ratios are shown in the top row of Fig. 5 for both non-prompt and prompt production in pp collisions at $\sqrt{s} = 5.02$ and 13 TeV. All the systematic uncertainties are propagated in the ratios treating them as correlated among different D-meson species, except for the ones related to the raw-yield extraction, the selection efficiency, the raw non-prompt fraction estimation, and the BR, which are treated as uncorrelated. While the prompt $D_s^+/(D^0 + D^+)$ ratio [14] indicates a hint of an increase with increasing p_T for p_T below 8 GeV/c, no significant dependence is visible for the strange-to-non-strange ratio for non-prompt mesons and no firm conclusions can be drawn given the current experimental uncertainties. Also, no significant dependence on \sqrt{s} is observed. This indicates that the ratios of fragmentation fractions of charm and beauty quarks into D mesons, as determined in pp collisions, exhibit no dependence on the collision energy, as detailed in Ref. [14]. The ratios are found to be compatible with those measured in e^+e^- collisions [86], indicating that the fragmentation fractions of heavy quarks into mesons are independent of the collision system. Note that this does not apply to the baryon sector, where noticeable differences have been observed between e^+e^- and pp (or p-Pb) collisions [14, 58, 68].

In the bottom panels of Fig. 5, the ratios of prompt and non-prompt D-meson cross sections measured at $\sqrt{s} = 13$ TeV are compared to the FONLL calculations for prompt D mesons and FONLL+PYTHIA 8 for the non-prompt ones. In the case of prompt D_s^+ mesons, no FONLL prediction is currently available. The theoretical predictions agree with the measured ratios in the p_T range of the analyses.

From the measured non-prompt $D_s^+/(D^0 + D^+)$ ratios, it is possible to compute the fragmentation fraction ratio of beauty quarks into strange (f_s) and non-strange (f_u and f_d) B mesons at a centre-of-mass energy of $\sqrt{s} = 13$ TeV. It is important to consider that a significant portion of the non-prompt D_s^+ mesons originates from decays of non-strange B mesons. Therefore, a correction factor is applied to the p_T -differential non-prompt $D_s^+/(D^0 + D^+)$ ratio. The correction factor is calculated from the FONLL+PYTHIA 8 predictions as

$$\alpha_{\text{corr.}}^{\text{FONLL+PYTHIA 8}} = \left[\frac{N(D_s^+ \leftarrow B_s^0)}{N(D_s^+ \leftarrow h_b)} \times \frac{N(D^0, D^+ \leftarrow h_b)}{N(D^0, D^+ \leftarrow B^{0,+})} \right]^{\text{FONLL+PYTHIA 8}}, \quad (2)$$

where $N(D_s^+ \leftarrow B_s^0)$ is the number of D_s^+ mesons produced in the decays of B_s^0 mesons, $N(D^0, D^+ \leftarrow B^{0,+})$ is the number of non-strange D mesons originating from non-strange B-meson decays, and $N(D_s^+ \leftarrow h_b)$ is the number of D_s^+ from beauty-hadron decays. The correction factor is found to be around 0.5. Given that the majority of the non-prompt D^0 and D^+ originate from non-strange B mesons, this indicates that about half of the non-prompt D_s^+ mesons originate from decays of strange B mesons.

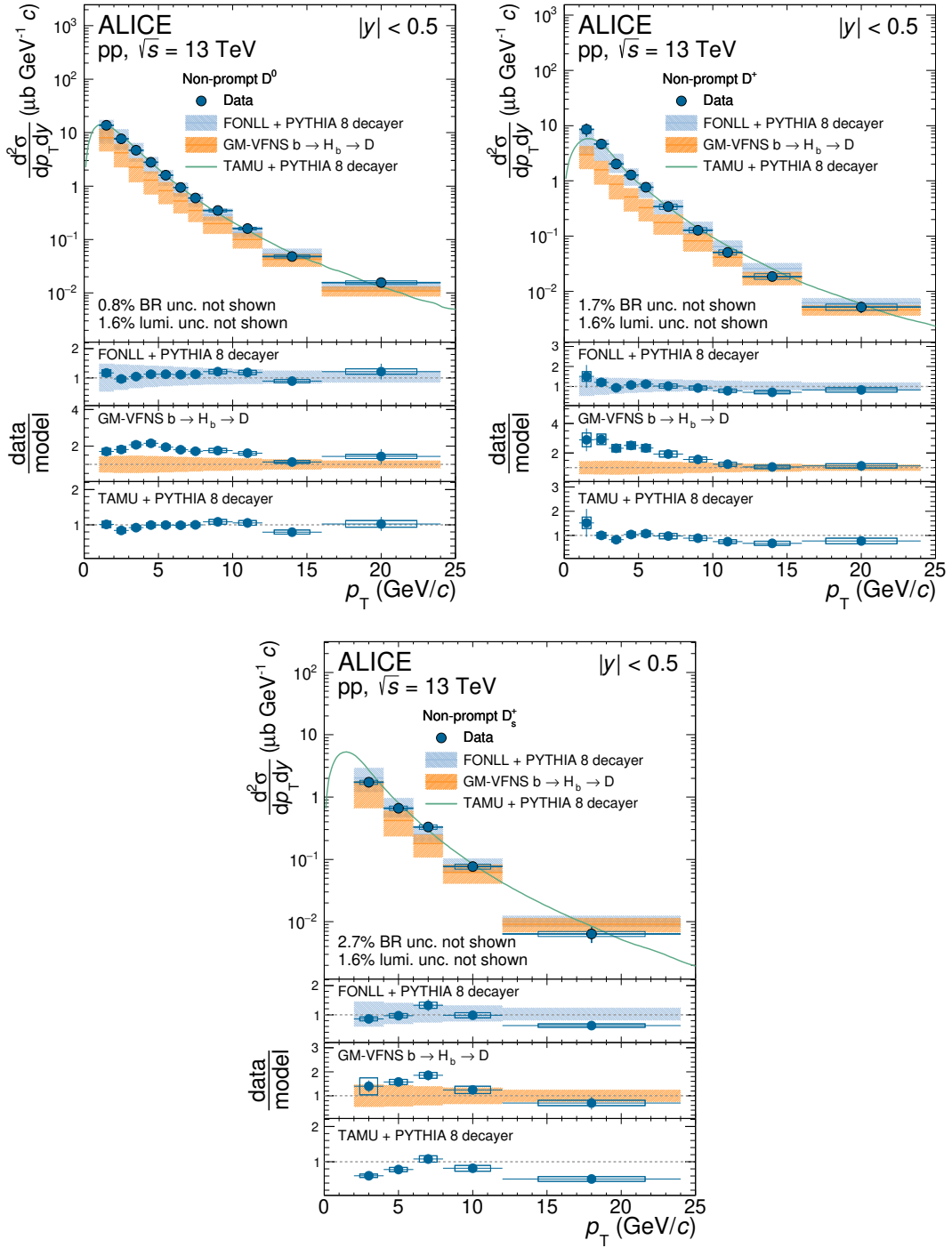


Figure 4: p_T -differential production cross sections of non-prompt D^0 (top-left), D^+ (top-right), and D_s^+ (bottom) mesons at midrapidity, $|y| < 0.5$, in pp collisions at $\sqrt{s} = 13$ TeV compared with the predictions from FONLL + PYTHIA 8 [47, 48], GM-VFNS [41, 42], and TAMU + PYTHIA 8 [82] calculations. The lower panels report the data-to-model ratios. The vertical bars and empty boxes represent the statistical and systematic uncertainties, respectively.

The ratio of the beauty-quark fragmentation fractions $f_s/(f_u + f_d)$ is computed as

$$\left(\frac{f_s}{f_u + f_d}\right)_{\text{beauty}} = \alpha_{\text{corr.}}^{\text{FONLL+PYTHIA 8}} \times \left(\frac{D_s^+}{D^0 + D^+}\right)_{\text{non-prompt}}, \quad (3)$$

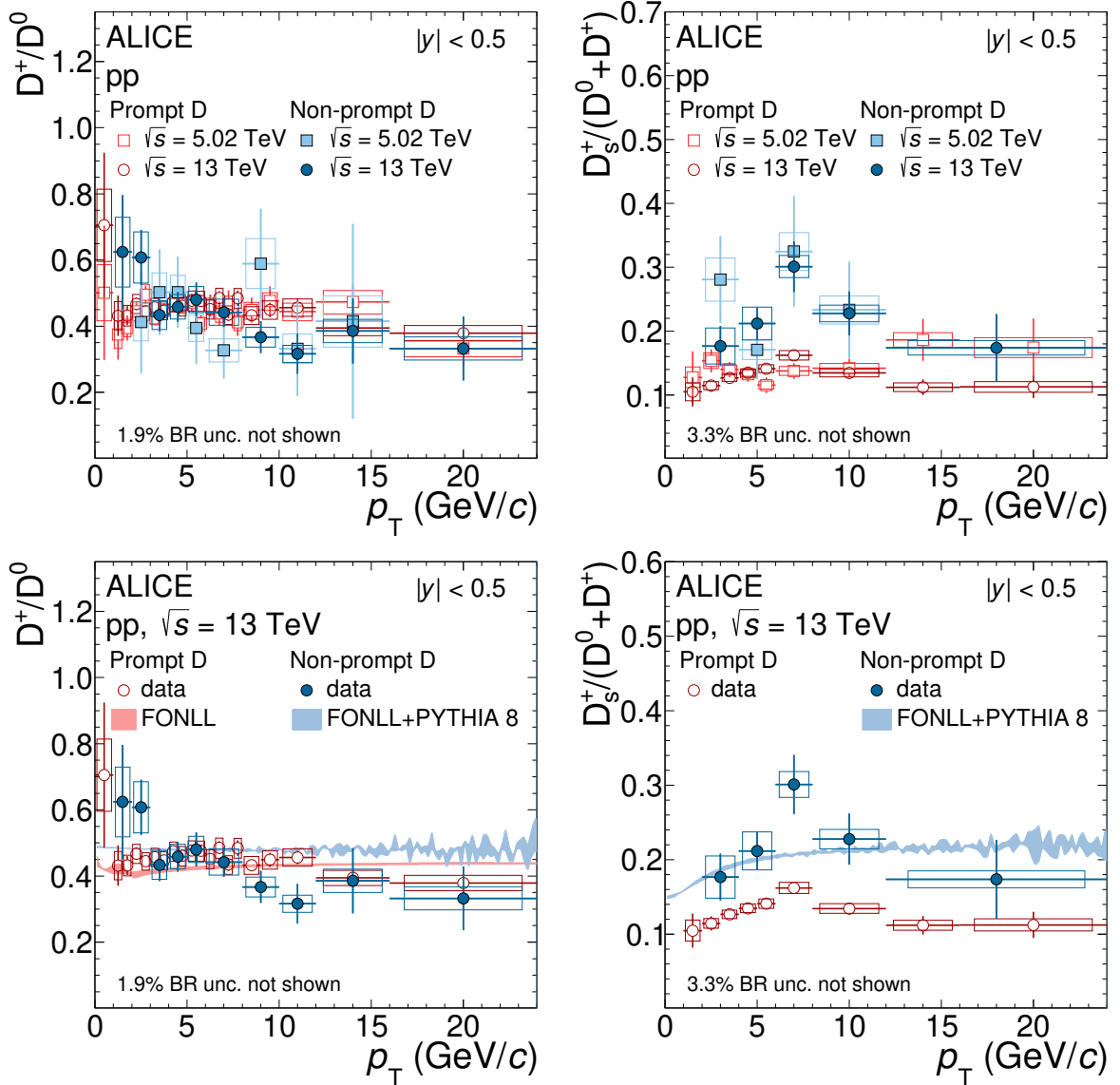


Figure 5: Top: ratios of prompt and non-prompt D-meson production cross sections as a function of p_T in pp collisions at $\sqrt{s} = 5.02$ [78] and 13 [14] TeV. Bottom: ratios of prompt [14] and non-prompt D-meson production cross sections as a function of p_T in pp collisions at $\sqrt{s} = 13$ TeV compared with FONLL+PYTHIA 8 predictions. The vertical bars and empty boxes report the statistical and systematic uncertainties, respectively.

where, in addition to the uncertainty related to the $D_s^+/(D^0 + D^+)$ measurement, the uncertainty on the correction factor $\alpha_{\text{corr.}}^{\text{FONLL+PYTHIA 8}}$ was considered. The latter was estimated by varying the beauty-quark fragmentation fractions and the branching ratios adopted for the $h_b \rightarrow D + X$ decays in PYTHIA 8.243 besides the uncertainties of FONLL, as discussed in detail in Ref. [78]. The ratio $f_s/(f_u + f_d)$ was calculated in the p_T intervals of the non-prompt $D_s^+/(D^0 + D^+)$ ratio measurement and it was found to be independent of p_T within the experimental uncertainties. It was fitted with a constant function to obtain the p_T -integrated fragmentation fraction. The result is:

$$\left(\frac{f_s}{f_u + f_d} \right)_{\text{beauty}} = 0.114 \pm 0.016 \text{ (stat.)} \pm 0.006 \text{ (syst.)} \pm 0.003 \text{ (BR)} \pm 0.003 \text{ (extrap.)}, \quad (4)$$

where “stat.” denotes the statistical uncertainty, “BR” is the uncertainty on the BR of the considered decays, and “extrap.” denotes the uncertainty due to the p_T extrapolation. The systematic uncertainty is denoted as “syst.” and it takes into account the yield extraction, track reconstruction and selection, D

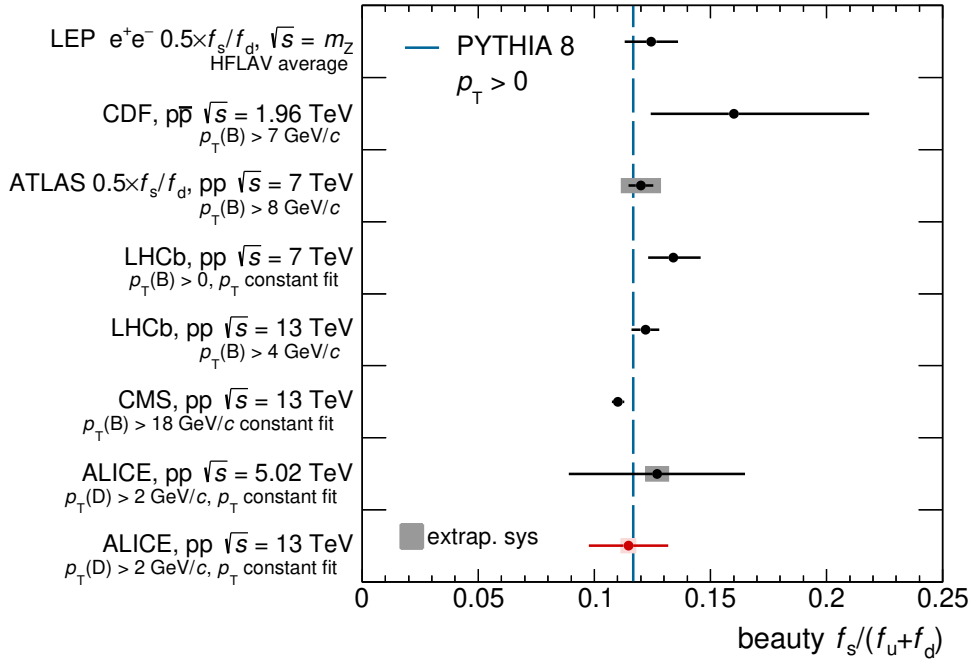


Figure 6: Beauty-quark fragmentation-fraction ratio $f_s/(f_u + f_d)$ calculated from non-prompt D-meson measurements in pp collisions at $\sqrt{s} = 13$ TeV compared with previous measurements from CDF [87], ALICE [78], ATLAS [17], CMS [19] and LHCb [57, 63], with the average of LEP measurements [86], and with the results of PYTHIA 8.243 simulations with Monash-13 tune [83].

meson selection, non-prompt fraction, and simulated p_T shape. In Fig. 6, the fragmentation fraction ratio is compared to previous measurements in pp and $p\bar{p}$ collisions at different \sqrt{s} values from the CDF [87], ALICE [78], ATLAS [17], and LHCb [57, 63] Collaborations. The ATLAS measurement of f_s/f_d was downscaled by a factor of two, assuming isospin symmetry for the u and d quarks (i.e. $f_u = f_d$). Figure 6 also shows that the beauty-quark fragmentation fractions extracted from the measurements in pp ($p\bar{p}$) collisions are compatible with those computed by the HFLAV Collaboration [86] using measurements in e^+e^- collisions at LEP. Similarly to the ATLAS measurement, the HFLAV results were scaled by a factor of two. The larger data sample collected by ALICE at $\sqrt{s} = 13$ TeV, compared to lower collision energies, enables a significant improvement in the precision of the measured beauty-quark fragmentation fraction ratio. Notably, the fragmentation fraction ratio for beauty quarks presented in this work is comparable to the one measured for charm quarks, which was determined to be 0.116 ± 0.011 (stat.) ± 0.009 (syst.) ± 0.003 (BR) [14] at a centre-of-mass energy of 13 TeV and 0.136 ± 0.005 (stat.) ± 0.006 (syst.) ± 0.005 (BR) [78] at 5.02 TeV. It is also consistent with the value of the strange to non-strange ratio for light-flavour particles predicted by the statistical hadronisation model [88], which is about 0.1, and with the outcome of PYTHIA 8.243 simulations with the Monash-13 tune [83].

To further explore the relationship of non-prompt D-meson production with the pp collision centre-of-mass energy, the ratios between the p_T -differential non-prompt D-meson cross sections at $\sqrt{s} = 13$ and 5.02 TeV [3, 78] were computed for D^0 , D^+ , and D_s^+ mesons. The results are shown in the left panel of Fig. 7. The systematic uncertainties were propagated treating them as uncorrelated between the two collision energies, with the exception of those related to the non-prompt fraction estimation and the branching ratio, which were treated as fully correlated. The ratios for the different D-meson species are compatible within the experimental uncertainties and share a common trend in p_T . The ratios hint at a common increase with increasing p_T , as also reported for charm-hadron ratios [14] and the equivalent ratio for B^+ mesons in the rapidity interval $2.0 < y < 4.5$ [26]. These findings suggest that there is a

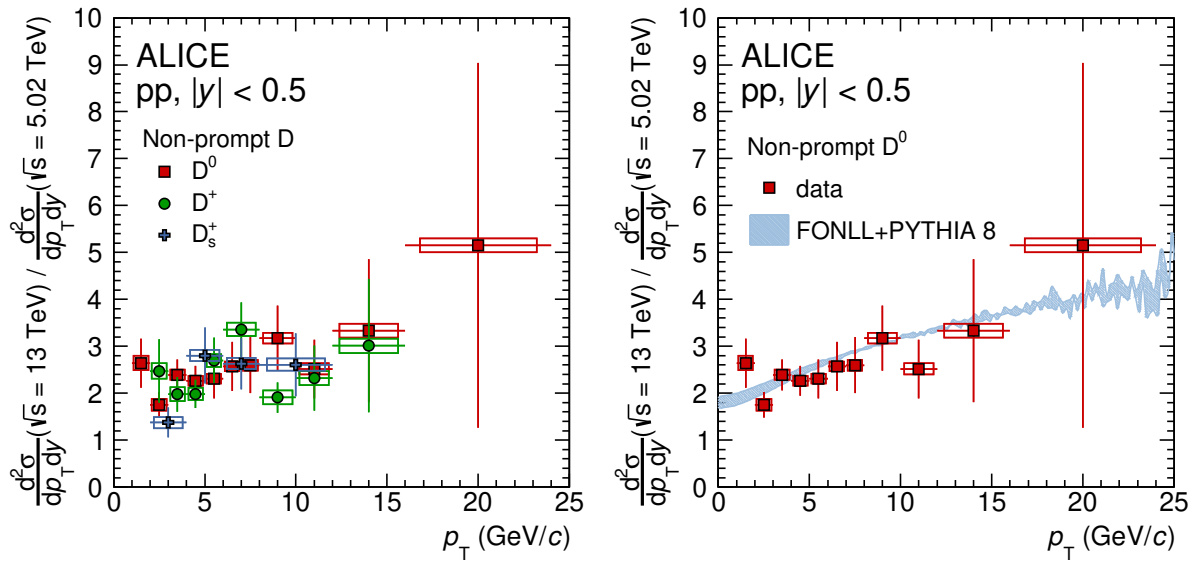


Figure 7: Ratios of non-prompt D-meson production cross sections at $\sqrt{s} = 13$ and 5.02 TeV [78] as a function of p_T . Left: comparison of measurements for D^0 , D^+ , and D_s^+ mesons. Right: comparison of D^0 results with FONLL+PYTHIA 8 calculations. The vertical bars and empty boxes report the statistical and systematic uncertainties, respectively.

similar hardening of the p_T -differential production cross section of heavy-flavour hadrons with increasing \sqrt{s} , which is independent of the species or origin of the hadron. In addition, a comparison was made between the measured 13-to-5.02 TeV ratio for non-prompt D^0 and the FONLL+PYTHIA 8 predictions, which is shown in the right panel of Fig. 7. The non-prompt D^0 results were chosen for this comparison due to the larger p_T coverage of the measurement and the higher precision compared to the other D meson species. The theoretical calculations also indicate an increasing trend of the non-prompt D^0 ratio as a function of p_T , and they reproduce the measurement within uncertainties. However, the current experimental uncertainties do not allow us to draw a firm conclusion on the dependence of the ratios on the D-meson p_T .

5.3 Beauty-quark production in pp collisions at $\sqrt{s} = 13$ TeV

The production cross section of $b\bar{b}$ pairs per unit of rapidity at midrapidity was computed independently for the non-prompt D^0 , D^+ , D_s^+ mesons, and Λ_c^+ baryons taken from Ref. [68] by combining two ingredients: (i) the measured visible cross sections for that specific species and (ii) the extrapolation factor to the $b\bar{b}$ -pair cross section ($\alpha_{\text{extrap}}^{b\bar{b}}$) taken from FONLL calculations. These two quantities were estimated following the procedure presented in Refs. [68, 78] and summarised below. Finally, the total $b\bar{b}$ cross section per unit of rapidity at midrapidity was estimated as the weighted average of the single $b\bar{b}$ cross sections of the various charm hadron species, h_c , adopting as weights the inverse of the quadratic sum of the absolute statistical and uncorrelated systematic uncertainties, encompassing the systematic uncertainty associated with the raw-yield extraction and the non-prompt fraction estimation.

The visible cross sections of the different non-prompt charm-hadron species were obtained by integrating the p_T -differential cross section in the measured p_T interval. In this calculation, the statistical uncertainty and the systematic uncertainty on the raw-yield extraction were treated as uncorrelated among the different p_T intervals. All the other sources were considered fully correlated. The extrapolation factor was computed for each measured non-prompt charm-hadron state from FONLL+PYTHIA 8 predictions, as the ratio of the beauty cross section and the visible cross sections of the measured non-prompt charm-hadron states in the p_T range of the analyses, as:

Table 2: Measured visible cross section ($d\sigma^{\text{vis.}}/dy|_{|y|<0.5}$), extrapolation factor ($\alpha_{\text{extrap.}}^{\text{bb}}$), and FONLL+PYTHIA 8 predictions of non-prompt charm-hadrons in pp collisions at $\sqrt{s} = 13$ TeV at midrapidity.

h_c	Kinematic range (GeV/c)	$d\sigma^{\text{vis.}}/dy _{ y <0.5}$ (μb)	$\alpha_{\text{extrap.}}^{\text{bb}}$	FONLL+PYTHIA 8 (μb)
D^0	$1 < p_T < 24$	33.3 ± 1.2 (stat.) ± 2.5 (syst.)	$1.241^{+0.009}_{-0.047}$	$30.7^{+13.7}_{-12.2}$
D^+	$1 < p_T < 24$	18.4 ± 2.4 (stat.) ± 2.3 (syst.)	$1.243^{+0.009}_{-0.048}$	$14.8^{+6.6}_{-5.9}$
D_s^+	$2 < p_T < 24$	5.8 ± 0.6 (stat.) ± 0.4 (syst.)	$1.858^{+0.037}_{-0.170}$	$6.3^{+2.7}_{-2.3}$
Λ_c^+ [68]	$2 < p_T < 24$	10.5 ± 1.3 (stat.) ± 0.9 (syst.)	$1.847^{+0.108}_{-0.152}$	$5.9^{+3.3}_{-2.4}$

$$\alpha_{\text{extrap.}}^{\text{bb}} = \frac{d\sigma_{\text{bb}}^{\text{FONLL}}/dy|_{|y|<0.5}}{d\sigma_{h_c \leftarrow b}^{\text{FONLL+PYTHIA 8}}/dy|_{|y|<0.5}(p_T^{\min h_c} < p_T < p_T^{\max h_c})}. \quad (5)$$

The systematic uncertainty on the extrapolation factor was determined by considering different sources of uncertainty including the ones associated with FONLL calculations, the uncertainties on the fragmentation fractions, and the uncertainties on the BR as was done for the estimation of the beauty-quark fragmentation fractions described in Section 5.2. Table 2 reports the kinematic range of the analyses together with the measured visible cross sections, the extrapolation factor, and the predictions of FONLL+PYTHIA 8 calculations for each non-prompt charm-hadron species [68].

Two additional corrections were considered, following the procedure of Refs [14, 68, 78]. The first correction factor accounts for the different rapidity distributions of beauty quarks and beauty hadrons, while the second correction accounts for the different rapidity distributions of $b\bar{b}$ pairs and beauty quarks. The first correction factor was estimated to be unity within the relevant rapidity range, based on FONLL calculations. An uncertainty of 1% was derived from the deviation between FONLL and PYTHIA 8.243. The second correction factor was computed from the rapidity distributions of b quarks and $b\bar{b}$ pairs obtained with POWHEG [89] simulations. The resulting value of the second correction factor is 1.06 ± 0.01 within the range $|y| < 0.5$, where the uncertainty was derived by varying the factorisation and renormalisation scales in the POWHEG calculation.

The measured $b\bar{b}$ production cross section per unit of rapidity at midrapidity in pp collisions at $\sqrt{s} = 13$ TeV is

$$\frac{d\sigma_{b\bar{b}}}{dy} \Big|_{|y|<0.5}^{\text{pp}, \sqrt{s}=13 \text{ TeV}} = 75.2 \pm 3.2(\text{stat.}) \pm 5.2(\text{syst.})^{+12.3}_{-3.2}(\text{extrap.}) \mu\text{b}, \quad (6)$$

where the uncertainty on the extrapolation of the cross section is reported separately and denoted as “extrap.”. The left panel of Fig. 8 reports a compilation of $b\bar{b}$ cross section measurements in pp collisions from the ALICE [9, 10, 50, 90–92] and PHENIX [30] Collaborations and in $p\bar{p}$ from the CDF [35] and UA1 [33] Collaborations, as a function of \sqrt{s} . The experimental results are compared with the predictions from FONLL and NNLO calculations. The measured $b\bar{b}$ cross sections and their dependence with \sqrt{s} are described by the pQCD calculations within the theoretical uncertainties, especially in the case of NNLO calculations that show smaller uncertainties compared to FONLL calculations. The central values of the NNLO calculations are closer to the data, as expected by the higher perturbative accuracy.

Finally, the dependence of the $b\bar{b}$ production cross section on the rapidity interval was investigated. The right panel of Fig. 8 reports the beauty cross section at midrapidity presented in this work, along with the measurements performed in pseudorapidity intervals by the LHCb Collaboration at forward rapidity [53].

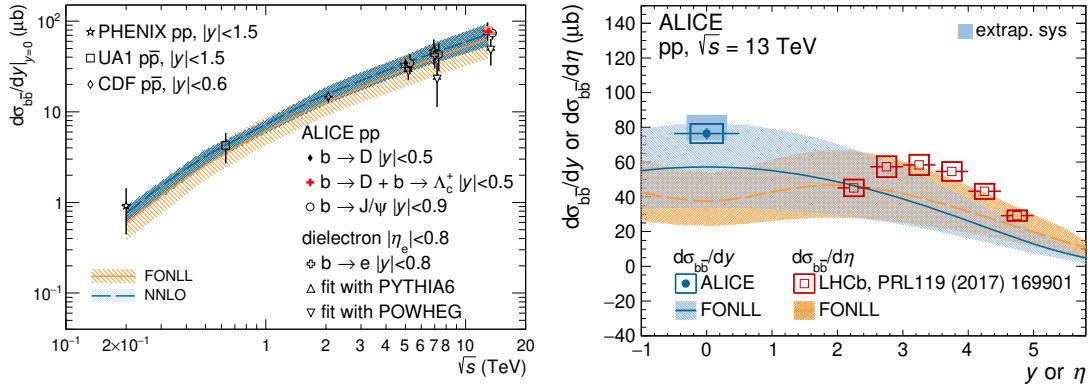


Figure 8: Left: beauty-quark production cross section per unit of rapidity at midrapidity as a function of the centre-of-mass energy measured in pp and $p\bar{p}$ collisions by the ALICE [9, 10, 50, 90–92] and PHENIX [30] Collaborations, and the CDF [35] and UA1 [33] Collaborations. The solid and dashed lines, accompanied by shaded bands, represent the central values and the associated uncertainties predicted by FONLL [47, 48, 93] and NNLO [94] calculations, respectively. Right: beauty-quark production cross section per unit of (pseudo)rapidity as a function of (pseudo)rapidity measured by the ALICE Collaboration (LHCb Collaboration [53]). The solid and dashed lines, accompanied by a shaded band, represent the central values and the associated uncertainties predicted by FONLL [47, 48, 93] as a function of y and η , respectively. The vertical bars and boxes report the statistical and systematic uncertainties, respectively.

The experimental results are compared to FONLL predictions, which are shown both for $d\sigma_{b\bar{b}}/dy$ and $d\sigma_{b\bar{b}}/d\eta$, to match the observables reported by ALICE and LHCb, respectively. The measured $b\bar{b}$ cross sections generally lie close to the upper boundary of the FONLL theoretical uncertainty band, except for the LHCb data point in $2 < \eta < 2.5$ which is compatible with the central value of the predictions.

6 Summary

The p_T -differential production cross sections of non-prompt D mesons were measured at midrapidity in pp collisions at $\sqrt{s} = 13$ TeV. The measurement of the non-prompt D^0 meson was performed in the $1 < p_T < 24$ GeV/ c range with a finer granularity in p_T compared to previously published measurements [68]. The measurements of the non-prompt D^+ and D_s^+ mesons were performed for the first time at this energy and cover the $1 < p_T < 24$ GeV/ c and $2 < p_T < 24$ GeV/ c ranges, respectively. The results were compared with FONLL and GM-VFNS pQCD calculations as well as with predictions from the TAMU model. A good agreement was found considering the current experimental uncertainties.

The non-prompt D^+/D^0 and $D_s^+/(D^0+D^+)$ p_T -differential production ratios were studied at $\sqrt{s} = 13$ TeV and were compared to the 5.02 TeV results. No significant dependence on the collision energy nor on the D-meson p_T was observed. A comparison was made with the predictions based on FONLL+PYTHIA 8, which describe the measured ratios well. These results were further employed to test the universality of the fragmentation function of beauty quarks in pp collisions by measuring the fraction of beauty quarks fragmenting into strange mesons relative to those fragmenting into non-strange mesons. The result is compatible with previously published measurements in e^+e^- , $p\bar{p}$, and pp collisions at different energies and with the analogous measurement in the charm sector [14]. Our results are consistent with the scenario in which the ratio of the fragmentation fraction of charm and beauty quarks into D mesons is universal, i.e. independent of the collision system and energy, even though violations of this universality are observed when considering heavy-flavour baryons [57–63]. In addition, the ratio of the non-prompt D meson production between $\sqrt{s} = 13$ and 5.02 TeV was measured for the three meson species. A hint of a common increase with increasing p_T was observed for all species, similar to what was already reported in analogous measurements of charm hadrons [14], even though the current experimental uncertainty

does not allow firm conclusions to be drawn. Predictions based on FONLL+PYTHIA 8 calculations qualitatively describe these ratios.

Finally, the total $b\bar{b}$ production cross section at midrapidity per unity of rapidity in pp collisions at $\sqrt{s} = 13$ TeV was determined. This result supersedes the previous measurement presented in Ref. [68] in terms of precision. The measured $b\bar{b}$ production cross section lies on the upper edge of the theoretical uncertainties of the predictions from FONLL and NNLO pQCD calculations.

Acknowledgements

The ALICE Collaboration would like to thank all its engineers and technicians for their invaluable contributions to the construction of the experiment and the CERN accelerator teams for the outstanding performance of the LHC complex. The ALICE Collaboration gratefully acknowledges the resources and support provided by all Grid centres and the Worldwide LHC Computing Grid (WLCG) collaboration. The ALICE Collaboration acknowledges the following funding agencies for their support in building and running the ALICE detector: A. I. Alikhanyan National Science Laboratory (Yerevan Physics Institute) Foundation (ANSL), State Committee of Science and World Federation of Scientists (WFS), Armenia; Austrian Academy of Sciences, Austrian Science Fund (FWF): [M 2467-N36] and Nationalstiftung für Forschung, Technologie und Entwicklung, Austria; Ministry of Communications and High Technologies, National Nuclear Research Center, Azerbaijan; Conselho Nacional de Desenvolvimento Científico e Tecnológico (CNPq), Financiadora de Estudos e Projetos (Finep), Fundação de Amparo à Pesquisa do Estado de São Paulo (FAPESP) and Universidade Federal do Rio Grande do Sul (UFRGS), Brazil; Bulgarian Ministry of Education and Science, within the National Roadmap for Research Infrastructures 2020-2027 (object CERN), Bulgaria; Ministry of Education of China (MOEC) , Ministry of Science & Technology of China (MSTC) and National Natural Science Foundation of China (NSFC), China; Ministry of Science and Education and Croatian Science Foundation, Croatia; Centro de Aplicaciones Tecnológicas y Desarrollo Nuclear (CEADEN), Cubaenergía, Cuba; Ministry of Education, Youth and Sports of the Czech Republic, Czech Republic; The Danish Council for Independent Research | Natural Sciences, the VILLUM FONDEN and Danish National Research Foundation (DNRF), Denmark; Helsinki Institute of Physics (HIP), Finland; Commissariat à l’Energie Atomique (CEA) and Institut National de Physique Nucléaire et de Physique des Particules (IN2P3) and Centre National de la Recherche Scientifique (CNRS), France; Bundesministerium für Bildung und Forschung (BMBF) and GSI Helmholtzzentrum für Schwerionenforschung GmbH, Germany; General Secretariat for Research and Technology, Ministry of Education, Research and Religions, Greece; National Research, Development and Innovation Office, Hungary; Department of Atomic Energy Government of India (DAE), Department of Science and Technology, Government of India (DST), University Grants Commission, Government of India (UGC) and Council of Scientific and Industrial Research (CSIR), India; National Research and Innovation Agency - BRIN, Indonesia; Istituto Nazionale di Fisica Nucleare (INFN), Italy; Japanese Ministry of Education, Culture, Sports, Science and Technology (MEXT) and Japan Society for the Promotion of Science (JSPS) KAKENHI, Japan; Consejo Nacional de Ciencia (CONACYT) y Tecnología, through Fondo de Cooperación Internacional en Ciencia y Tecnología (FONCICYT) and Dirección General de Asuntos del Personal Académico (DGAPA), Mexico; Nederlandse Organisatie voor Wetenschappelijk Onderzoek (NWO), Netherlands; The Research Council of Norway, Norway; Commission on Science and Technology for Sustainable Development in the South (COMSATS), Pakistan; Pontificia Universidad Católica del Perú, Peru; Ministry of Education and Science, National Science Centre and WUT ID-UB, Poland; Korea Institute of Science and Technology Information and National Research Foundation of Korea (NRF), Republic of Korea; Ministry of Education and Scientific Research, Institute of Atomic Physics, Ministry of Research and Innovation and Institute of Atomic Physics and Universitatea Nationala de Stiinta si Tehnologie Politehnica Bucuresti, Romania; Ministry of Education, Science, Research and Sport of the Slovak

Republic, Slovakia; National Research Foundation of South Africa, South Africa; Swedish Research Council (VR) and Knut & Alice Wallenberg Foundation (KAW), Sweden; European Organization for Nuclear Research, Switzerland; Suranaree University of Technology (SUT), National Science and Technology Development Agency (NSTDA) and National Science, Research and Innovation Fund (NSRF via PMU-B B05F650021), Thailand; Turkish Energy, Nuclear and Mineral Research Agency (TENMAK), Turkey; National Academy of Sciences of Ukraine, Ukraine; Science and Technology Facilities Council (STFC), United Kingdom; National Science Foundation of the United States of America (NSF) and United States Department of Energy, Office of Nuclear Physics (DOE NP), United States of America. In addition, individual groups or members have received support from: Czech Science Foundation (grant no. 23-07499S), Czech Republic; European Research Council (grant no. 950692), European Union; ICSC - Centro Nazionale di Ricerca in High Performance Computing, Big Data and Quantum Computing, European Union - NextGenerationEU; Academy of Finland (Center of Excellence in Quark Matter) (grant nos. 346327, 346328), Finland.

References

- [1] F. Prino and R. Rapp, “Open Heavy Flavor in QCD Matter and in Nuclear Collisions”, *J. Phys. G* **43** (2016) 093002, arXiv:1603.00529 [nucl-ex].
- [2] ALICE Collaboration, B. Abelev *et al.*, “Measurement of charm production at central rapidity in proton-proton collisions at $\sqrt{s} = 2.76$ TeV”, *JHEP* **07** (2012) 191, arXiv:1205.4007 [hep-ex].
- [3] ALICE Collaboration, S. Acharya *et al.*, “Measurement of D^0 , D^+ , D^{*+} and D_s^+ production in pp collisions at $\sqrt{s} = 5.02$ TeV with ALICE”, *Eur. Phys. J. C* **79** (2019) 388, arXiv:1901.07979 [nucl-ex].
- [4] ALICE Collaboration, S. Acharya *et al.*, “Measurement of D-meson production at mid-rapidity in pp collisions at $\sqrt{s} = 7$ TeV”, *Eur. Phys. J. C* **77** (2017) 550, arXiv:1702.00766 [hep-ex].
- [5] ALICE Collaboration, B. Abelev *et al.*, “ D_s^+ meson production at central rapidity in proton-proton collisions at $\sqrt{s} = 7$ TeV”, *Phys. Lett. B* **718** (2012) 279–294, arXiv:1208.1948 [hep-ex].
- [6] ALICE Collaboration, B. Abelev *et al.*, “Production of muons from heavy flavour decays at forward rapidity in pp and Pb–Pb collisions at $\sqrt{s_{NN}} = 2.76$ TeV”, *Phys. Rev. Lett.* **109** (2012) 112301, arXiv:1205.6443 [hep-ex].
- [7] ALICE Collaboration, B. Abelev *et al.*, “Heavy flavour decay muon production at forward rapidity in proton-proton collisions at $\sqrt{s} = 7$ TeV”, *Phys. Lett. B* **708** (2012) 265–275, arXiv:1201.3791 [hep-ex].
- [8] ALICE Collaboration, B. Abelev *et al.*, “Beauty production in pp collisions at $\sqrt{s} = 2.76$ TeV measured via semi-electronic decays”, *Phys. Lett. B* **738** (2014) 97–108, arXiv:1405.4144 [nucl-ex].
- [9] ALICE Collaboration, B. Abelev *et al.*, “Measurement of prompt J/ψ and beauty hadron production cross sections at mid-rapidity in pp collisions at $\sqrt{s} = 7$ TeV”, *JHEP* **11** (2012) 065, arXiv:1205.5880 [hep-ex].
- [10] ALICE Collaboration, S. Acharya *et al.*, “Dielectron production in proton-proton collisions at $\sqrt{s} = 7$ TeV”, *JHEP* **09** (2018) 064, arXiv:1805.04391 [hep-ex].
- [11] ALICE Collaboration, S. Acharya *et al.*, “Measurement of electrons from semileptonic heavy-flavour hadron decays at midrapidity in pp and Pb–Pb collisions at $\sqrt{s_{NN}} = 5.02$ TeV”, *Phys. Lett. B* **804** (2020) 135377, arXiv:1910.09110 [nucl-ex].

- [12] **ALICE** Collaboration, S. Acharya *et al.*, “Production of muons from heavy-flavour hadron decays in pp collisions at $\sqrt{s} = 5.02$ TeV”, *JHEP* **09** (2019) 008, arXiv:1905.07207 [nucl-ex].
- [13] **ALICE** Collaboration, S. Acharya *et al.*, “The ALICE experiment: a journey through QCD”, *Eur. Phys. J. C* **84** (2024) 813, arXiv:2211.04384 [nucl-ex].
- [14] **ALICE** Collaboration, S. Acharya *et al.*, “Charm production and fragmentation fractions at midrapidity in pp collisions at $\sqrt{s} = 13$ TeV”, *JHEP* **12** (2023) 086, arXiv:2308.04877 [hep-ex].
- [15] **ATLAS** Collaboration, G. Aad *et al.*, “Measurement of $D^{*\pm}$, D^\pm and D_s^\pm meson production cross sections in pp collisions at $\sqrt{s} = 7$ TeV with the ATLAS detector”, *Nucl. Phys. B* **907** (2016) 717–763, arXiv:1512.02913 [hep-ex].
- [16] **ATLAS** Collaboration, G. Aad *et al.*, “Measurement of the differential cross-section of B^+ meson production in pp collisions at $\sqrt{s} = 7$ TeV at ATLAS”, *JHEP* **10** (2013) 042, arXiv:1307.0126 [hep-ex].
- [17] **ATLAS** Collaboration, G. Aad *et al.*, “Determination of the ratio of b -quark fragmentation fractions f_s/f_d in pp collisions at $\sqrt{s} = 7$ TeV with the ATLAS detector”, *Phys. Rev. Lett.* **115** (2015) 262001, arXiv:1507.08925 [hep-ex].
- [18] **CMS** Collaboration, A. Tumasyan *et al.*, “Measurement of prompt open-charm production cross sections in proton-proton collisions at $\sqrt{s} = 13$ TeV”, *JHEP* **11** (2021) 225, arXiv:2107.01476 [hep-ex].
- [19] **CMS** Collaboration, A. Tumasyan *et al.*, “Measurement of the dependence of the hadron production fraction ratios f_s/f_u and f_d/f_u on b meson kinematic variables in proton-proton collisions at $\sqrt{s} = 13$ TeV”, *Phys. Rev. Lett.* **131** (Sep, 2023) 121901. <https://link.aps.org/doi/10.1103/PhysRevLett.131.121901>.
- [20] **CMS** Collaboration, S. Chatrchyan *et al.*, “Measurement of the Strange B Meson Production Cross Section with $J/\Psi \phi$ Decays in pp Collisions at $\sqrt{s} = 7$ TeV”, *Phys. Rev. D* **84** (2011) 052008, arXiv:1106.4048 [hep-ex].
- [21] **CMS** Collaboration, S. Chatrchyan *et al.*, “Measurement of the B^0 production cross section in pp Collisions at $\sqrt{s} = 7$ TeV”, *Phys. Rev. Lett.* **106** (2011) 252001, arXiv:1104.2892 [hep-ex].
- [22] **CMS** Collaboration, S. Chatrchyan *et al.*, “Measurement of the Λ_b Cross Section and the $\bar{\Lambda}_b$ to Λ_b Ratio with $J/\Psi \Lambda$ Decays in pp Collisions at $\sqrt{s} = 7$ TeV”, *Phys. Lett. B* **714** (2012) 136–157, arXiv:1205.0594 [hep-ex].
- [23] **LHCb** Collaboration, R. Aaij *et al.*, “Prompt charm production in pp collisions at $\sqrt{s} = 7$ TeV”, *Nucl. Phys. B* **871** (2013) 1–20, arXiv:1302.2864 [hep-ex].
- [24] **LHCb** Collaboration, R. Aaij *et al.*, “Measurements of prompt charm production cross-sections in pp collisions at $\sqrt{s} = 13$ TeV”, *JHEP* **03** (2016) 159, arXiv:1510.01707 [hep-ex]. [Erratum: *JHEP* **09**, 013 (2016), Erratum: *JHEP* **05**, 074 (2017)].
- [25] **LHCb** Collaboration, R. Aaij *et al.*, “Measurements of prompt charm production cross-sections in pp collisions at $\sqrt{s} = 5$ TeV”, *JHEP* **06** (2017) 147, arXiv:1610.02230 [hep-ex].
- [26] **LHCb** Collaboration, R. Aaij *et al.*, “Measurement of the B^\pm production cross-section in pp collisions at $\sqrt{s} = 7$ and 13 TeV”, *JHEP* **12** (2017) 026, arXiv:1710.04921 [hep-ex].

- [27] **LHCb** Collaboration, R. Aaij *et al.*, “Study of the production of Λ_b^0 and \bar{B}^0 hadrons in pp collisions and first measurement of the $\Lambda_b^0 \rightarrow J/\psi p K^-$ branching fraction”, *Chin. Phys. C* **40** (2016) 011001, arXiv:1509.00292 [hep-ex].
- [28] **LHCb** Collaboration, R. Aaij *et al.*, “First Measurement of Charm Production in its Fixed-Target Configuration at the LHC”, *Phys. Rev. Lett.* **122** (2019) 132002, arXiv:1810.07907 [hep-ex].
- [29] **PHENIX** Collaboration, A. Adare *et al.*, “Measurement of high- p_T single electrons from heavy-flavor decays in $p + p$ collisions at $\sqrt{s} = 200$ GeV”, *Phys. Rev. Lett.* **97** (2006) 252002, arXiv:hep-ex/0609010.
- [30] **PHENIX** Collaboration, A. Adare *et al.*, “Measurement of Bottom versus Charm as a Function of Transverse Momentum with Electron-Hadron Correlations in pp Collisions at $\sqrt{s} = 200$ GeV”, *Phys. Rev. Lett.* **103** (2009) 082002, arXiv:0903.4851 [hep-ex].
- [31] **STAR** Collaboration, L. Adamczyk *et al.*, “Measurements of D^0 and D^* Production in $p + p$ Collisions at $\sqrt{s} = 200$ GeV”, *Phys. Rev. D* **86** (2012) 072013, arXiv:1204.4244 [nucl-ex].
- [32] **PHENIX** Collaboration, A. Adare *et al.*, “Measurements of e^+e^- pairs from open heavy flavor in $p+p$ and $d+A$ collisions at $\sqrt{s_{NN}} = 200$ GeV”, *Phys. Rev. C* **96** (2017) 024907, arXiv:1702.01084 [nucl-ex].
- [33] **UA1** Collaboration, C. Albajar *et al.*, “Beauty production at the CERN $p\bar{p}$ collider”, *Phys. Lett. B* **256** (1991) 121–128. [Erratum: *Phys.Lett.B* 262, 497 (1991)].
- [34] **CDF** Collaboration, D. Acosta *et al.*, “Measurement of prompt charm meson production cross sections in $p\bar{p}$ collisions at $\sqrt{s} = 1.96$ TeV”, *Phys. Rev. Lett.* **91** (2003) 241804, arXiv:hep-ex/0307080.
- [35] **CDF** Collaboration, D. Acosta *et al.*, “Measurement of the J/ψ meson and b -hadron production cross sections in $p\bar{p}$ collisions at $\sqrt{s} = 1960$ GeV”, *Phys. Rev. D* **71** (2005) 032001, arXiv:hep-ex/0412071.
- [36] **CDF** Collaboration, A. Abulencia *et al.*, “Measurement of the B^+ production cross-section in p anti-p collisions at $\sqrt{s} = 1960$ GeV”, *Phys. Rev. D* **75** (2007) 012010, arXiv:hep-ex/0612015.
- [37] **CDF** Collaboration, T. Aaltonen *et al.*, “Measurement of the b-Hadron Production Cross Section Using Decays to $\mu^- D^0 X$ Final States in p anti-p Collisions at $\sqrt{s} = 1.96$ TeV”, *Phys. Rev. D* **79** (2009) 092003, arXiv:0903.2403 [hep-ex].
- [38] J. C. Collins, D. E. Soper, and G. F. Sterman, “Factorization of Hard Processes in QCD”, *Adv. Ser. Direct. High Energy Phys.* **5** (1989) 1–91, arXiv:hep-ph/0409313.
- [39] T. Kneesch, B. A. Kniehl, G. Kramer, and I. Schienbein, “Charmed-meson fragmentation functions with finite-mass corrections”, *Nucl. Phys. B* **799** (2008) 34–59, arXiv:0712.0481 [hep-ph].
- [40] B. A. Kniehl and G. Kramer, “Charmed-hadron fragmentation functions from CERN LEP1 revisited”, *Phys. Rev. D* **74** (2006) 037502, arXiv:hep-ph/0607306.
- [41] M. Benzke, M. V. Garzelli, B. Kniehl, G. Kramer, S. Moch, and G. Sigl, “Prompt neutrinos from atmospheric charm in the general-mass variable-flavor-number scheme”, *JHEP* **12** (2017) 021, arXiv:1705.10386 [hep-ph].

- [42] G. Kramer and H. Spiesberger, “Study of heavy meson production in p–Pb collisions at $\sqrt{s} = 5.02$ TeV in the general-mass variable-flavour-number scheme”, *Nucl. Phys. B* **925** (2017) 415–430, arXiv:1703.04754 [hep-ph].
- [43] B. A. Kniehl, G. Kramer, I. Schienbein, and H. Spiesberger, “Inclusive D^{*+} production in p anti-p collisions with massive charm quarks”, *Phys. Rev. D* **71** (2005) 014018, arXiv:hep-ph/0410289.
- [44] B. A. Kniehl, G. Kramer, I. Schienbein, and H. Spiesberger, “Collinear subtractions in hadroproduction of heavy quarks”, *Eur. Phys. J. C* **41** (2005) 199–212, arXiv:hep-ph/0502194.
- [45] B. A. Kniehl, G. Kramer, I. Schienbein, and H. Spiesberger, “Inclusive Charmed-Meson Production at the CERN LHC”, *Eur. Phys. J. C* **72** (2012) 2082, arXiv:1202.0439 [hep-ph].
- [46] I. Helenius and H. Paukkunen, “Revisiting the D-meson hadroproduction in general-mass variable flavour number scheme”, *JHEP* **05** (2018) 196, arXiv:1804.03557 [hep-ph].
- [47] M. Cacciari, M. Greco, and P. Nason, “The p_T spectrum in heavy flavor hadroproduction”, *JHEP* **05** (1998) 007, arXiv:hep-ph/9803400.
- [48] M. Cacciari, S. Frixione, N. Houdeau, M. L. Mangano, P. Nason, and G. Ridolfi, “Theoretical predictions for charm and bottom production at the LHC”, *JHEP* **10** (2012) 137, arXiv:1205.6344 [hep-ph].
- [49] CMS Collaboration, V. Khachatryan *et al.*, “Prompt and Non-Prompt J/ψ Production in pp Collisions at $\sqrt{s} = 7$ TeV”, *Eur. Phys. J. C* **71** (2011) 1575, arXiv:1011.4193 [hep-ex].
- [50] ALICE Collaboration, B. Abelev *et al.*, “Measurement of electrons from beauty hadron decays in pp collisions at $\sqrt{s} = 7$ TeV”, *Phys. Lett. B* **721** (2013) 13–23, arXiv:1208.1902 [hep-ex]. [Erratum: Phys.Lett.B 763, 507–509 (2016)].
- [51] CMS Collaboration, V. Khachatryan *et al.*, “Measurement of the total and differential inclusive B^+ hadron cross sections in pp collisions at $\sqrt{s} = 13$ TeV”, *Phys. Lett. B* **771** (2017) 435–456, arXiv:1609.00873 [hep-ex].
- [52] LHCb Collaboration, R. Aaij *et al.*, “Measurement of forward J/ψ production cross-sections in pp collisions at $\sqrt{s} = 13$ TeV”, *JHEP* **10** (2015) 172, arXiv:1509.00771 [hep-ex]. [Erratum: JHEP 05, 063 (2017)].
- [53] LHCb Collaboration, R. Aaij *et al.*, “Measurement of the b -quark production cross-section in 7 and 13 TeV pp collisions”, *Phys. Rev. Lett.* **118** (2017) 052002, arXiv:1612.05140 [hep-ex]. [Erratum: Phys.Rev.Lett. 119, 169901 (2017)].
- [54] ALICE Collaboration, S. Acharya *et al.*, “Inclusive and multiplicity dependent production of electrons from heavy-flavour hadron decays in pp and p–Pb collisions”, *JHEP* **08** (2023) 006, arXiv:2303.13349 [nucl-ex].
- [55] LHCb Collaboration, R. Aaij *et al.*, “Observation of strangeness enhancement with charmed mesons in high-multiplicity pPb collisions at $\sqrt{s_{NN}} = 8.16$ TeV”, arXiv:2311.08490 [hep-ex].
- [56] LHCb Collaboration, R. Aaij *et al.*, “Evidence for modification of b quark hadronization in high-multiplicity pp collisions at $\sqrt{s} = 13$ TeV”, *Phys. Rev. Lett.* **131** (2023) 061901, arXiv:2204.13042 [hep-ex].
- [57] LHCb Collaboration, R. Aaij *et al.*, “Measurement of b -hadron production fractions in 7 TeV pp collisions”, *Phys. Rev. D* **85** (2012) 032008, arXiv:1111.2357 [hep-ex].




















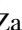






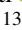


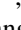







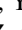
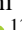
- [58] **ALICE** Collaboration, S. Acharya *et al.*, “ Λ_c^+ Production and Baryon-to-Meson Ratios in pp and p–Pb Collisions at $\sqrt{s_{NN}} = 5.02$ TeV at the LHC”, *Phys. Rev. Lett.* **127** (2021) 202301, arXiv:2011.06078 [nucl-ex].
- [59] **ALICE** Collaboration, S. Acharya *et al.*, “ Λ_c^+ production in pp and in p–Pb collisions at $\sqrt{s_{NN}} = 5.02$ TeV”, *Phys. Rev. C* **104** (2021) 054905, arXiv:2011.06079 [nucl-ex].
- [60] **ALICE** Collaboration, S. Acharya *et al.*, “First measurement of Λ_c^+ production down to $p_T = 0$ in pp and p–Pb collisions at $\sqrt{s_{NN}} = 5.02$ TeV”, *Phys. Rev. C* **107** (2023) 064901, arXiv:2211.14032 [nucl-ex].
- [61] **ALICE** Collaboration, S. Acharya *et al.*, “Measurement of Prompt D^0 , Λ_c^+ , and $\Sigma_c^{0,++}(2455)$ Production in Proton–Proton Collisions at $\sqrt{s} = 13$ TeV”, *Phys. Rev. Lett.* **128** (2022) 012001, arXiv:2106.08278 [hep-ex].
- [62] **ALICE** Collaboration, S. Acharya *et al.*, “Measurement of the Cross Sections of Ξ_c^0 and Ξ_c^+ Baryons and of the Branching-Fraction Ratio $\text{BR}(\Xi_c^0 \rightarrow \Xi^- e^+ \nu_e)/\text{BR}(\Xi_c^0 \rightarrow \Xi^- \pi^+)$ in pp collisions at 13 TeV”, *Phys. Rev. Lett.* **127** (2021) 272001, arXiv:2105.05187 [nucl-ex].
- [63] **LHCb** Collaboration, R. Aaij *et al.*, “Measurement of b hadron fractions in 13 TeV pp collisions”, *Phys. Rev. D* **100** (2019) 031102, arXiv:1902.06794 [hep-ex].
- [64] **CMS** Collaboration, A. M. Sirunyan *et al.*, “Production of Λ_c^+ baryons in proton-proton and lead-lead collisions at $\sqrt{s_{NN}} = 5.02$ TeV”, *Phys. Lett. B* **803** (2020) 135328, arXiv:1906.03322 [hep-ex].
- [65] **OPAL** Collaboration, G. Alexander *et al.*, “A study of charm hadron production in $Z^0 \rightarrow c\bar{c}$ and $Z^0 \rightarrow b\bar{b}$ decays at LEP”, *Z. Phys. C* **72** (1996) 1–16.
- [66] S. Frixione, P. Nason, and G. Ridolfi, “A Positive-weight next-to-leading-order Monte Carlo for heavy flavour hadroproduction”, *JHEP* **09** (2007) 126, arXiv:0707.3088 [hep-ph].
- [67] T. Sjostrand, S. Mrenna, and P. Z. Skands, “PYTHIA 6.4 Physics and Manual”, *JHEP* **05** (2006) 026, arXiv:hep-ph/0603175.
- [68] **ALICE** Collaboration, S. Acharya *et al.*, “Study of flavor dependence of the baryon-to-meson ratio in proton-proton collisions at $\sqrt{s} = 13$ TeV”, *Phys. Rev. D* **108** (2023) 112003, arXiv:2308.04873 [hep-ex].
- [69] **ALICE** Collaboration, K. Aamodt *et al.*, “The ALICE experiment at the CERN LHC”, *JINST* **3** (2008) S08002.
- [70] **ALICE** Collaboration, B. Abelev *et al.*, “Performance of the ALICE Experiment at the CERN LHC”, *Int. J. Mod. Phys. A* **29** (2014) 1430044, arXiv:1402.4476 [nucl-ex].
- [71] **ALICE** Collaboration, S. Acharya *et al.*, “ALICE 2016-2017-2018 luminosity determination for pp collisions at $\sqrt{s} = 13$ TeV”, <https://cds.cern.ch/record/2776672>.
- [72] T. Sjöstrand, S. Ask, J. R. Christiansen, R. Corke, N. Desai, P. Ilten, S. Mrenna, S. Prestel, C. O. Rasmussen, and P. Z. Skands, “An introduction to PYTHIA 8.2”, *Comput. Phys. Commun.* **191** (2015) 159–177, arXiv:1410.3012 [hep-ph].
- [73] R. Brun, F. Bruyant, F. Carminati, S. Giani, M. Maire, A. McPherson, G. Patrick, and L. Urban, *GEANT: Detector Description and Simulation Tool; Oct 1994*. CERN Program Library. CERN, Geneva, 1993. <https://cds.cern.ch/record/1082634>. Long Writeup W5013.

- [74] **Particle Data Group** Collaboration, R. L. Workman *et al.*, “Review of Particle Physics”, *PTEP* **2022** (2022) 083C01.
- [75] **ALICE** Collaboration, S. Acharya *et al.*, “First measurement of prompt and non-prompt D^{*+} vector meson spin alignment in pp collisions at $\sqrt{s} = 13$ TeV”, *Phys. Lett. B* **846** (2023) 137920, arXiv:2212.06588 [nucl-ex].
- [76] T. Chen and C. Guestrin, “XGBoost: A scalable tree boosting system”, in *Proceedings of the 22nd ACM SIGKDD International Conference on Knowledge Discovery and Data Mining*, KDD ’16, p. 785–794. Association for Computing Machinery, New York, NY, USA, 2016. <https://doi.org/10.1145/2939672.2939785>.
- [77] L. Barioglio, F. Catalano, M. Concas, P. Fecchio, F. Grosa, F. Mazzaschi, and M. Puccio, “hipe4ml/hipe4ml”, Apr., 2022. <https://doi.org/10.5281/zenodo.7014886>.
- [78] **ALICE** Collaboration, S. Acharya *et al.*, “Measurement of beauty and charm production in pp collisions at $\sqrt{s} = 5.02$ TeV via non-prompt and prompt D mesons”, *JHEP* **05** (2021) 220, arXiv:2102.13601 [nucl-ex].
- [79] **ALICE** Collaboration, S. Acharya *et al.*, “Measurement of beauty-strange meson production in Pb–Pb collisions at $\sqrt{s_{NN}} = 5.02$ TeV via non-prompt D_s^+ mesons”, *Phys. Lett. B* **846** (2023) 137561, arXiv:2204.10386 [nucl-ex].
- [80] S. M. Lundberg and S.-I. Lee, “A unified approach to interpreting model predictions”, in *Advances in Neural Information Processing Systems 30*, pp. 4765–4774. 2017. <https://arxiv.org/abs/1705.07874>.
- [81] P. Bolzoni and G. Kramer, “Inclusive charmed-meson production from bottom hadron decays at the LHC”, *J. Phys. G* **41** (2014) 075006, arXiv:1310.2924 [hep-ph].
- [82] M. He and R. Rapp, “Bottom hadrochemistry in high-energy hadronic collisions”, *Phys. Rev. Lett.* **131** (Jul, 2023) 012301. <https://link.aps.org/doi/10.1103/PhysRevLett.131.012301>.
- [83] P. Skands, S. Carrazza, and J. Rojo, “Tuning PYTHIA 8.1: the Monash 2013 Tune”, *Eur. Phys. J. C* **74** (2014) 3024, arXiv:1404.5630 [hep-ph].
- [84] J. Pumplin, D. R. Stump, J. Huston, H. L. Lai, P. M. Nadolsky, and W. K. Tung, “New generation of parton distributions with uncertainties from global QCD analysis”, *JHEP* **07** (2002) 012, arXiv:hep-ph/0201195.
- [85] S. Dulat, T.-J. Hou, J. Gao, *et al.*, “New parton distribution functions from a global analysis of quantum chromodynamics”, *Phys. Rev. D* **93** (2016) 033006, arXiv:1506.07443 [hep-ph].
- [86] **Heavy Flavor Averaging Group** Collaboration, Y. S. Amhis *et al.*, “Averages of b-hadron, c-hadron, and τ -lepton properties as of 2021”, *Phys. Rev. D* **107** (2023) 052008, arXiv:2206.07501 [hep-ex].
- [87] **CDF** Collaboration, T. Aaltonen *et al.*, “Measurement of ratios of fragmentation fractions for bottom hadrons in $p\bar{p}$ collisions at $\sqrt{s} = 1.96$ TeV”, *Phys. Rev. D* **77** (2008) 072003, arXiv:0801.4375 [hep-ex].
- [88] P. Braun-Munzinger, J. Cleymans, H. Oeschler, and K. Redlich, “Maximum relative strangeness content in heavy ion collisions around 30 GeV/A”, *Nucl. Phys. A* **697** (2002) 902–912, arXiv:hep-ph/0106066.

- [89] S. Alioli, P. Nason, C. Oleari, and E. Re, “A general framework for implementing NLO calculations in shower Monte Carlo programs: the POWHEG BOX”, *JHEP* **06** (2010) 043, arXiv:1002.2581 [hep-ph].
- [90] ALICE Collaboration, S. Acharya *et al.*, “Prompt and non-prompt J/ψ production cross sections at midrapidity in proton-proton collisions at $\sqrt{s} = 5.02$ and 13 TeV”, *JHEP* **03** (2022) 190, arXiv:2108.02523 [nucl-ex].
- [91] ALICE Collaboration, S. Acharya *et al.*, “Dielectron and heavy-quark production in inelastic and high-multiplicity proton-proton collisions at $\sqrt{s_{NN}} = 13$ TeV”, *Phys. Lett. B* **788** (2019) 505–518, arXiv:1805.04407 [hep-ex].
- [92] ALICE Collaboration, S. Acharya *et al.*, “Dielectron production in proton-proton and proton-lead collisions at $\sqrt{s_{NN}} = 5.02$ TeV”, *Phys. Rev. C* **102** (2020) 055204, arXiv:2005.11995 [nucl-ex].
- [93] M. Cacciari, S. Frixione, and P. Nason, “The p_T spectrum in heavy flavor photoproduction”, *JHEP* **03** (2001) 006, arXiv:hep-ph/0102134.
- [94] S. Catani, S. Devoto, M. Grazzini, S. Kallweit, and J. Mazzitelli, “Bottom-quark production at hadron colliders: fully differential predictions in NNLO QCD”, *JHEP* **03** (2021) 029, arXiv:2010.11906 [hep-ph].

F. Grosa ³³, J.F. Grosse-Oetringhaus ³³, R. Grosso ⁹⁸, D. Grund ³⁶, N.A. Grunwald ⁹⁵,
G.G. Guardiano ¹¹², R. Guernane ⁷⁴, M. Guilbaud ¹⁰⁴, K. Gulbrandsen ⁸⁴, T. Gündem ⁶⁵, T. Gunji ¹²⁵,
W. Guo ⁶, A. Gupta ⁹², R. Gupta ⁹², R. Gupta ⁴⁹, K. Gwizdzziel ¹³⁷, L. Gyulai ⁴⁷, C. Hadjidakis ¹³²,
F.U. Haider ⁹², S. Haidlova ³⁶, M. Haldar ⁴, H. Hamagaki ⁷⁷, A. Hamdi ⁷⁵, Y. Han ¹⁴⁰, B.G. Hanley ¹³⁸,
R. Hannigan ¹⁰⁹, J. Hansen ⁷⁶, M.R. Haque ⁹⁸, J.W. Harris ¹³⁹, A. Harton ⁹, M.V. Hartung ⁶⁵,
H. Hassan ¹¹⁸, D. Hatzifotiadou ⁵², P. Hauer ⁴³, L.B. Havener ¹³⁹, E. Hellbär ⁹⁸, H. Helstrup ³⁵,
M. Hemmer ⁶⁵, T. Herman ³⁶, S.G. Hernandez ¹¹⁷, G. Herrera Corral ⁸, F. Herrmann ¹²⁷, S. Herrmann ¹²⁹,
K.F. Hetland ³⁵, B. Heybeck ⁶⁵, H. Hillemanns ³³, B. Hippolyte ¹³⁰, F.W. Hoffmann ⁷¹, B. Hofman ⁶⁰,
G.H. Hong ¹⁴⁰, M. Horst ⁹⁶, A. Horzyk ², Y. Hou ⁶, P. Hristov ³³, P. Huhn ⁶⁵, L.M. Huhta ¹¹⁸,
T.J. Humanic ⁸⁹, A. Hutson ¹¹⁷, D. Hutter ³⁹, M.C. Hwang ¹⁹, R. Ilkaev ¹⁴², H. Ilyas ¹⁴, M. Inaba ¹²⁶,
G.M. Innocenti ³³, M. Ippolitov ¹⁴², A. Isakov ⁸⁵, T. Isidori ¹¹⁹, M.S. Islam ¹⁰⁰, M. Ivanov ⁹⁸,
M. Ivanov ¹³, V. Ivanov ¹⁴², K.E. Iversen ⁷⁶, M. Jablonski ², B. Jacak ^{19,75}, N. Jacazio ²⁶,
P.M. Jacobs ⁷⁵, S. Jadlovská ¹⁰⁷, J. Jadlovsky ¹⁰⁷, S. Jaelani ⁸³, C. Jahnke ¹¹¹, M.J. Jakubowska ¹³⁷,
M.A. Janik ¹³⁷, T. Janson ⁷¹, S. Ji ¹⁷, S. Jia ¹⁰, T. Jiang ¹⁰, A.A.P. Jimenez ⁶⁶, F. Jonas ^{75,88,127},
D.M. Jones ¹²⁰, J.M. Jowett ^{33,98}, J. Jung ⁶⁵, M. Jung ⁶⁵, A. Junique ³³, A. Jusko ¹⁰¹, J. Kaewjai ¹⁰⁶,
P. Kalinak ⁶¹, A. Kalweit ³³, A. Karasu Uysal ^{V,73}, D. Karatovic ⁹⁰, O. Karavichev ¹⁴²,
T. Karavicheva ¹⁴², E. Karpechev ¹⁴², M.J. Karwowska ^{33,137}, U. Kebschull ⁷¹, R. Keidel ¹⁴¹,
D.L.D. Keijndener ⁶⁰, M. Keil ³³, B. Ketzer ⁴³, S.S. Khade ⁴⁹, A.M. Khan ¹²¹, S. Khan ¹⁶,
A. Khanzadeev ¹⁴², Y. Kharlov ¹⁴², A. Khatun ¹¹⁹, A. Khuntia ³⁶, Z. Khuranova ⁶⁵, B. Kileng ³⁵,
B. Kim ¹⁰⁵, C. Kim ¹⁷, D.J. Kim ¹¹⁸, E.J. Kim ⁷⁰, J. Kim ¹⁴⁰, J. Kim ⁵⁹, J. Kim ⁷⁰, M. Kim ¹⁹,
S. Kim ¹⁸, T. Kim ¹⁴⁰, K. Kimura ⁹³, A. Kirkova ³⁷, S. Kirsch ⁶⁵, I. Kisel ³⁹, S. Kiselev ¹⁴²,
A. Kisiel ¹³⁷, J.P. Kitowski ², J.L. Klay ⁵, J. Klein ³³, S. Klein ⁷⁵, C. Klein-Bösing ¹²⁷, M. Kleiner ⁶⁵,
T. Klemenz ⁹⁶, A. Kluge ³³, C. Kobdaj ¹⁰⁶, R. Kohara ¹²⁵, T. Kollegger ⁹⁸, A. Kondratyev ¹⁴³,
N. Kondratyeva ¹⁴², J. König ⁶⁵, S.A. Königstorfer ⁹⁶, P.J. Konopka ³³, G. Kornakov ¹³⁷,
M. Korwieser ⁹⁶, S.D. Koryciak ², A. Kotliarov ⁸⁷, N. Kovacic ⁹⁰, V. Kovalenko ¹⁴², M. Kowalski ¹⁰⁸,
V. Kozuharov ³⁷, I. Králik ⁶¹, A. Kravčáková ³⁸, L. Krcal ^{33,39}, M. Krivda ^{101,61}, F. Krizek ⁸⁷,
K. Krizkova Gajdosova ³³, C. Krug ⁶⁷, M. Krüger ⁶⁵, D.M. Krupova ³⁶, E. Kryshen ¹⁴², V. Kučera ⁵⁹,
C. Kuhn ¹³⁰, P.G. Kuijper ⁸⁵, T. Kumaoka ¹²⁶, D. Kumar ¹³⁶, L. Kumar ⁹¹, N. Kumar ⁹¹, S. Kumar ³²,
S. Kundu ³³, P. Kurashvili ⁸⁰, A. Kurepin ¹⁴², A.B. Kurepin ¹⁴², A. Kuryakin ¹⁴², S. Kushpil ⁸⁷,
V. Kuskov ¹⁴², M. Kutyla ¹³⁷, M.J. Kweon ⁵⁹, Y. Kwon ¹⁴⁰, S.L. La Pointe ³⁹, P. La Rocca ²⁷,
A. Lakrathok ¹⁰⁶, M. Lamanna ³³, A.R. Landou ⁷⁴, R. Langoy ¹²², P. Larionov ³³, E. Laudi ³³,
L. Lautner ^{33,96}, R.A.N. Laveaga ¹¹⁰, R. Lavicka ¹⁰³, R. Lea ^{135,56}, H. Lee ¹⁰⁵, I. Legrand ⁴⁶,
G. Legras ¹²⁷, J. Lehrbach ³⁹, T.M. Lelek ², R.C. Lemmon ⁸⁶, I. León Monzón ¹¹⁰, M.M. Lesch ⁹⁶,
E.D. Lesser ¹⁹, P. Lévai ⁴⁷, X. Li ¹⁰, B.E. Liang-gilman ¹⁹, J. Lien ¹²², R. Lietava ¹⁰¹, I. Likmeta ¹¹⁷,
B. Lim ²⁵, S.H. Lim ¹⁷, V. Lindenstruth ³⁹, A. Lindner ⁴⁶, C. Lippmann ⁹⁸, D.H. Liu ⁶, J. Liu ¹²⁰,
G.S.S. Liveraro ¹¹², I.M. Lofnes ²¹, C. Loizides ⁸⁸, S. Lokos ¹⁰⁸, J. Lömker ⁶⁰, P. Loncar ³⁴,
X. Lopez ¹²⁸, E. López Torres ⁷, P. Lu ^{98,121}, F.V. Lugo ⁶⁸, J.R. Luhder ¹²⁷, M. Lunardon ²⁸,
G. Luparello ⁵⁸, Y.G. Ma ⁴⁰, M. Mager ³³, A. Maire ¹³⁰, E.M. Majerz ², M.V. Makariev ³⁷,
M. Malaev ¹⁴², G. Malfattore ²⁶, N.M. Malik ⁹², Q.W. Malik ²⁰, S.K. Malik ⁹², L. Malinina ^{I,VIII,143},
D. Mallick ¹³², N. Mallick ⁴⁹, G. Mandaglio ^{31,54}, S.K. Mandal ⁸⁰, A. Manea ⁶⁴, V. Manko ¹⁴²,
F. Manso ¹²⁸, V. Manzari ⁵¹, Y. Mao ⁶, R.W. Marcjan ², G.V. Margagliotti ²⁴, A. Margotti ⁵²,
A. Marín ⁹⁸, C. Markert ¹⁰⁹, P. Martinengo ³³, M.I. Martínez ⁴⁵, G. Martínez García ¹⁰⁴,
M.P.P. Martins ¹¹¹, S. Masciocchi ⁹⁸, M. Masera ²⁵, A. Masoni ⁵³, L. Massacrier ¹³², O. Massen ⁶⁰,
A. Mastroserio ^{133,51}, O. Matonoha ⁷⁶, S. Mattiazzo ²⁸, A. Matyja ¹⁰⁸, A.L. Mazuecos ³³,
F. Mazzaschi ²⁵, M. Mazzilli ³³, J.E. Mdhliu ¹²⁴, Y. Melikyan ⁴⁴, A. Menchaca-Rocha ⁶⁸,
J.E.M. Mendez ⁶⁶, E. Meninno ¹⁰³, A.S. Menon ¹¹⁷, M.W. Menzel ^{33,95}, M. Meres ¹³, Y. Miake ¹²⁶,
L. Micheletti ³³, D.L. Mihaylov ⁹⁶, K. Mikhaylov ^{143,142}, N. Minafra ¹¹⁹, D. Miśkowiec ⁹⁸,
A. Modak ⁴, B. Mohanty ⁸¹, M. Mohisin Khan ^{VI,16}, M.A. Molander ⁴⁴, S. Monira ¹³⁷, C. Mordasini ¹¹⁸,
D.A. Moreira De Godoy ¹²⁷, I. Morozov ¹⁴², A. Morsch ³³, T. Mrnjavac ³³, V. Muccifora ⁵⁰,
S. Muhuri ¹³⁶, J.D. Mulligan ⁷⁵, A. Mulliri ²³, M.G. Munhoz ¹¹¹, R.H. Munzer ⁶⁵, H. Murakami ¹²⁵,
S. Murray ¹¹⁵, L. Musa ³³, J. Musinsky ⁶¹, J.W. Myrcha ¹³⁷, B. Naik ¹²⁴, A.I. Nambrath ¹⁹,
B.K. Nandi ⁴⁸, R. Nania ⁵², E. Nappi ⁵¹, A.F. Nassirpour ¹⁸, A. Nath ⁹⁵, C. Nattrass ¹²³,
M.N. Naydenov ³⁷, A. Neagu ²⁰, A. Negru ¹¹⁴, E. Nekrasova ¹⁴², L. Nellen ⁶⁶, R. Nepeivoda ⁷⁶, S. Nese ²⁰,
G. Neskovic ³⁹, N. Nicassio ⁵¹, B.S. Nielsen ⁸⁴, E.G. Nielsen ⁸⁴, S. Nikolaev ¹⁴², S. Nikulin ¹⁴²,
V. Nikulin ¹⁴², F. Noferini ⁵², S. Noh ¹², P. Nomokonov ¹⁴³, J. Norman ¹²⁰, N. Novitzky ⁸⁸,
P. Nowakowski ¹³⁷, A. Nyanin ¹⁴², J. Nystrand ²¹, S. Oh ¹⁸, A. Ohlson ⁷⁶, V.A. Okorokov ¹⁴²,

J. Oleniacz¹³⁷, A. Onnerstad¹¹⁸, C. Oppedisano⁵⁷, A. Ortiz Velasquez⁶⁶, J. Otwinowski¹⁰⁸, M. Oya⁹³, K. Oyama⁷⁷, Y. Pachmayer⁹⁵, S. Padhan⁴⁸, D. Pagano^{135,56}, G. Paic⁶⁶, S. Paisano-Guzmán⁴⁵, A. Palasciano⁵¹, S. Panebianco¹³¹, H. Park¹²⁶, H. Park¹⁰⁵, J.E. Parkkila³³, Y. Patley⁴⁸, B. Paul²³, M.M.D.M. Paulino¹¹¹, H. Pei⁶, T. Peitzmann⁶⁰, X. Peng¹¹, M. Pennisi²⁵, S. Perciballi²⁵, D. Peresunko¹⁴², G.M. Perez⁷, Y. Pestov¹⁴², V. Petrov¹⁴², M. Petrovici⁴⁶, R.P. Pezzi^{104,67}, S. Piano⁵⁸, M. Pikna¹³, P. Pillot¹⁰⁴, O. Pinazza^{52,33}, L. Pinsky¹¹⁷, C. Pinto⁹⁶, S. Pisano⁵⁰, M. Płoskoń⁷⁵, M. Planinic⁹⁰, F. Pliquett⁶⁵, M.G. Poghosyan⁸⁸, B. Polichtchouk¹⁴², S. Politano³⁰, N. Poljak⁹⁰, A. Pop⁴⁶, S. Porteboeuf-Houssais¹²⁸, V. Pozdniakov¹⁴³, I.Y. Pozos⁴⁵, K.K. Pradhan⁴⁹, S.K. Prasad⁴, S. Prasad⁴⁹, R. Preghenella⁵², F. Prino⁵⁷, C.A. Pruneau¹³⁸, I. Pshenichnov¹⁴², M. Puccio³³, S. Pucillo²⁵, S. Qiu⁸⁵, L. Quaglia²⁵, S. Ragoni¹⁵, A. Rai¹³⁹, A. Rakotozafindrabe¹³¹, L. Ramello^{134,57}, F. Rami¹³⁰, M. Rasa²⁷, S.S. Räsänen⁴⁴, R. Rath⁵², M.P. Rauch²¹, I. Ravasenga³³, K.F. Read^{88,123}, C. Reckziegel¹¹³, A.R. Redelbach³⁹, K. Redlich^{7,80}, C.A. Reetz⁹⁸, H.D. Regules-Medel⁴⁵, A. Rehman²¹, F. Reidt³³, H.A. Reme-Ness³⁵, Z. Rescakova³⁸, K. Reygers⁹⁵, A. Riabov¹⁴², V. Riabov¹⁴², R. Ricci²⁹, M. Richter²¹, A.A. Riedel⁹⁶, W. Riegler³³, A.G. Riffero²⁵, C. Ripoli²⁹, C. Ristea⁶⁴, M.V. Rodriguez³³, M. Rodríguez Cahuantzi⁴⁵, S.A. Rodríguez Ramírez⁴⁵, K. Røed²⁰, R. Rogalev¹⁴², E. Rogochaya¹⁴³, T.S. Rogoschinski⁶⁵, D. Rohr³³, D. Röhrich²¹, S. Rojas Torres³⁶, P.S. Rokita¹³⁷, G. Romanenko²⁶, F. Ronchetti⁵⁰, E.D. Rosas⁶⁶, K. Roslon¹³⁷, A. Rossi⁵⁵, A. Roy⁴⁹, S. Roy⁴⁸, N. Rubini²⁶, D. Ruggiano¹³⁷, R. Rui²⁴, P.G. Russek², R. Russo⁸⁵, A. Rustamov⁸², E. Ryabinkin¹⁴², Y. Ryabov¹⁴², A. Rybicki¹⁰⁸, J. Ryu¹⁷, W. Rzesza¹³⁷, O.A.M. Saarimaki⁴⁴, S. Sadhu³², S. Sadovsky¹⁴², J. Saetre²¹, K. Šafařík³⁶, S.K. Saha⁴, S. Saha⁸¹, B. Sahoo⁴⁹, R. Sahoo⁴⁹, S. Sahoo⁶², D. Sahu⁴⁹, P.K. Sahu⁶², J. Saini¹³⁶, K. Sajdakova³⁸, S. Sakai¹²⁶, M.P. Salvan⁹⁸, S. Sambyal⁹², D. Samitz¹⁰³, I. Sanna^{33,96}, T.B. Saramela¹¹¹, D. Sarkar⁸⁴, P. Sarma⁴², V. Sarritzu²³, V.M. Sarti⁹⁶, M.H.P. Sas³³, S. Sawan⁸¹, E. Scapparone⁵², J. Schambach⁸⁸, H.S. Scheid⁶⁵, C. Schiaua⁴⁶, R. Schicker⁹⁵, F. Schlepfer⁹⁵, A. Schmah⁹⁸, C. Schmidt⁹⁸, H.R. Schmidt⁹⁴, M.O. Schmidt³³, M. Schmidt⁹⁴, N.V. Schmidt⁸⁸, A.R. Schmier¹²³, R. Schotter¹³⁰, A. Schröter³⁹, J. Schukraft³³, K. Schweda⁹⁸, G. Scioli²⁶, E. Scomparin⁵⁷, J.E. Seger¹⁵, Y. Sekiguchi¹²⁵, D. Sekihata¹²⁵, M. Selina⁸⁵, I. Selyuzhenkov⁹⁸, S. Senyukov¹³⁰, J.J. Seo⁹⁵, D. Serebryakov¹⁴², L. Serkin⁶⁶, L. Šerkšnytė⁹⁶, A. Sevcenco⁶⁴, T.J. Shaba⁶⁹, A. Shabetai¹⁰⁴, R. Shahoyan³³, A. Shangaraev¹⁴², B. Sharma⁹², D. Sharma⁴⁸, H. Sharma⁵⁵, M. Sharma⁹², S. Sharma⁷⁷, S. Sharma⁹², U. Sharma⁹², A. Shatat¹³², O. Sheibani¹¹⁷, K. Shigaki⁹³, M. Shimomura⁷⁸, J. Shin¹², S. Shirinkin¹⁴², Q. Shou⁴⁰, Y. Sibiriak¹⁴², S. Siddhanta⁵³, T. Siemiarczuk⁸⁰, T.F. Silva¹¹¹, D. Silvermyr⁷⁶, T. Simantathammakul¹⁰⁶, R. Simeonov³⁷, B. Singh⁹², B. Singh⁹⁶, K. Singh⁴⁹, R. Singh⁸¹, R. Singh⁹², R. Singh^{98,49}, S. Singh¹⁶, V.K. Singh¹³⁶, V. Singhal¹³⁶, T. Sinha¹⁰⁰, B. Sitar¹³, M. Sitta^{134,57}, T.B. Skaali²⁰, G. Skorodumovs⁹⁵, N. Smirnov¹³⁹, R.J.M. Snellings⁶⁰, E.H. Solheim²⁰, J. Song¹⁷, C. Sonnabend^{33,98}, J.M. Sonneveld⁸⁵, F. Soramel²⁸, A.B. Soto-hernandez⁸⁹, R. Spijkers⁸⁵, I. Sputowska¹⁰⁸, J. Staa⁷⁶, J. Stachel⁹⁵, I. Stan⁶⁴, P.J. Steffanic¹²³, S.F. Stiefelmaier⁹⁵, D. Stocco¹⁰⁴, I. Storehaug²⁰, N.J. Strangmann⁶⁵, P. Stratmann¹²⁷, S. Strazzi²⁶, A. Sturmiolo^{31,54}, C.P. Stylianidis⁸⁵, A.A.P. Suaide¹¹¹, C. Suire¹³², M. Sukhanov¹⁴², M. Suljic³³, R. Sultanov¹⁴², V. Sumberia⁹², S. Sumowidagdo⁸³, I. Szarka¹³, M. Szymkowski¹³⁷, S.F. Taghavi⁹⁶, G. Taillepied⁹⁸, J. Takahashi¹¹², G.J. Tambave⁸¹, S. Tang⁶, Z. Tang¹²¹, J.D. Tapia Takaki¹¹⁹, N. Tapus¹¹⁴, L.A. Tarasovicova¹²⁷, M.G. Tazila⁴⁶, G.F. Tassielli³², A. Tauro³³, A. Tavira García¹³², G. Tejeda Muñoz⁴⁵, A. Telesca³³, L. Terlizzi²⁵, C. Terrevoli⁵¹, S. Thakur⁴, D. Thomas¹⁰⁹, A. Tikhonov¹⁴², N. Tiltmann^{33,127}, A.R. Timmins¹¹⁷, M. Tkacik¹⁰⁷, T. Tkacik¹⁰⁷, A. Toia⁶⁵, R. Tokumoto⁹³, S. Tomassini²⁶, K. Tomohiro⁹³, N. Topilskaya¹⁴², M. Toppi⁵⁰, T. Tork¹³², V.V. Torres¹⁰⁴, A.G. Torres Ramos³², A. Trifiró^{31,54}, A.S. Triolo^{33,31,54}, S. Tripathy⁵², T. Tripathy⁴⁸, V. Trubnikov³, W.H. Trzaska¹¹⁸, T.P. Trzcinski¹³⁷, A. Tumkin¹⁴², R. Turrisi⁵⁵, T.S. Tveter²⁰, K. Ullaland²¹, B. Ulukutlu⁹⁶, A. Uras¹²⁹, M. Urioni¹³⁵, G.L. Usai²³, M. Vala³⁸, N. Valle⁵⁶, L.V.R. van Doremalen⁶⁰, M. van Leeuwen⁸⁵, C.A. van Veen⁹⁵, R.J.G. van Weelden⁸⁵, P. Vande Vyvre³³, D. Varga⁴⁷, Z. Varga⁴⁷, P. Vargas Torres⁶⁶, M. Vasileiou⁷⁹, A. Vasiliev¹⁴², O. Vázquez Doce⁵⁰, O. Vazquez Rueda¹¹⁷, V. Vechernin¹⁴², E. Vercellin²⁵, S. Vergara Limón⁴⁵, R. Verma⁴⁸, L. Vermunt⁹⁸, R. Vértesi⁴⁷, M. Verweij⁶⁰, L. Vickovic³⁴, Z. Vilakazi¹²⁴, O. Villalobos Baillie¹⁰¹, A. Villani²⁴, A. Vinogradov¹⁴², T. Virgili²⁹, M.M.O. Virta¹¹⁸, V. Vislavicius⁷⁶, A. Vodopyanov¹⁴³, B. Volkel³³, M.A. Völkl⁹⁵, S.A. Voloshin¹³⁸, G. Volpe³², B. von Haller³³, I. Vorobyev³³, N. Vozniuk¹⁴², J. Vrláková³⁸, J. Wan⁴⁰, C. Wang⁴⁰, D. Wang⁴⁰, Y. Wang⁴⁰, Y. Wang⁶, A. Wegrzynek³³, F.T. Weiglhofer³⁹, S.C. Wenzel³³, J.P. Wessels¹²⁷, J. Wiechula⁶⁵,

J. Wikne ²⁰, G. Wilk ⁸⁰, J. Wilkinson ⁹⁸, G.A. Willems ¹²⁷, B. Windelband ⁹⁵, M. Winn ¹³¹, J.R. Wright ¹⁰⁹, W. Wu⁴⁰, Y. Wu ¹²¹, Z. Xiong¹²¹, R. Xu ⁶, A. Yadav ⁴³, A.K. Yadav ¹³⁶, S. Yalcin ⁷³, Y. Yamaguchi ⁹³, S. Yang²¹, S. Yano ⁹³, E.R. Yeats¹⁹, Z. Yin ⁶, I.-K. Yoo ¹⁷, J.H. Yoon ⁵⁹, H. Yu¹², S. Yuan²¹, A. Yuncu ⁹⁵, V. Zaccolo ²⁴, C. Zampolli ³³, M. Zang⁶, F. Zanone ⁹⁵, N. Zardoshti ³³, A. Zarochentsev ¹⁴², P. Závada ⁶³, N. Zaviyalov¹⁴², M. Zhalov ¹⁴², B. Zhang ⁶, C. Zhang ¹³¹, L. Zhang ⁴⁰, M. Zhang ⁶, S. Zhang ⁴⁰, X. Zhang ⁶, Y. Zhang¹²¹, Z. Zhang ⁶, M. Zhao ¹⁰, V. Zhrebchevskii ¹⁴², Y. Zhi¹⁰, C. Zhong⁴⁰, D. Zhou ⁶, Y. Zhou ⁸⁴, J. Zhu ^{55,6}, Y. Zhu⁶, S.C. Zugeravel ⁵⁷, N. Zurlo ^{135,56}

Affiliation Notes

^I Deceased

^{II} Also at: Max-Planck-Institut für Physik, Munich, Germany

^{III} Also at: Italian National Agency for New Technologies, Energy and Sustainable Economic Development (ENEA), Bologna, Italy

^{IV} Also at: Dipartimento DET del Politecnico di Torino, Turin, Italy

^V Also at: Yildiz Technical University, Istanbul, Türkiye

^{VI} Also at: Department of Applied Physics, Aligarh Muslim University, Aligarh, India

^{VII} Also at: Institute of Theoretical Physics, University of Wrocław, Poland

^{VIII} Also at: An institution covered by a cooperation agreement with CERN

Collaboration Institutes

¹ A.I. Alikhanyan National Science Laboratory (Yerevan Physics Institute) Foundation, Yerevan, Armenia

² AGH University of Krakow, Cracow, Poland

³ Bogolyubov Institute for Theoretical Physics, National Academy of Sciences of Ukraine, Kiev, Ukraine

⁴ Bose Institute, Department of Physics and Centre for Astroparticle Physics and Space Science (CAPSS), Kolkata, India

⁵ California Polytechnic State University, San Luis Obispo, California, United States

⁶ Central China Normal University, Wuhan, China

⁷ Centro de Aplicaciones Tecnológicas y Desarrollo Nuclear (CEADEN), Havana, Cuba

⁸ Centro de Investigación y de Estudios Avanzados (CINVESTAV), Mexico City and Mérida, Mexico

⁹ Chicago State University, Chicago, Illinois, United States

¹⁰ China Institute of Atomic Energy, Beijing, China

¹¹ China University of Geosciences, Wuhan, China

¹² Chungbuk National University, Cheongju, Republic of Korea

¹³ Comenius University Bratislava, Faculty of Mathematics, Physics and Informatics, Bratislava, Slovak Republic

¹⁴ COMSATS University Islamabad, Islamabad, Pakistan

¹⁵ Creighton University, Omaha, Nebraska, United States

¹⁶ Department of Physics, Aligarh Muslim University, Aligarh, India

¹⁷ Department of Physics, Pusan National University, Pusan, Republic of Korea

¹⁸ Department of Physics, Sejong University, Seoul, Republic of Korea

¹⁹ Department of Physics, University of California, Berkeley, California, United States

²⁰ Department of Physics, University of Oslo, Oslo, Norway

²¹ Department of Physics and Technology, University of Bergen, Bergen, Norway

²² Dipartimento di Fisica, Università di Pavia, Pavia, Italy

²³ Dipartimento di Fisica dell'Università and Sezione INFN, Cagliari, Italy

²⁴ Dipartimento di Fisica dell'Università and Sezione INFN, Trieste, Italy

²⁵ Dipartimento di Fisica dell'Università and Sezione INFN, Turin, Italy

²⁶ Dipartimento di Fisica e Astronomia dell'Università and Sezione INFN, Bologna, Italy

²⁷ Dipartimento di Fisica e Astronomia dell'Università and Sezione INFN, Catania, Italy

²⁸ Dipartimento di Fisica e Astronomia dell'Università and Sezione INFN, Padova, Italy

²⁹ Dipartimento di Fisica 'E.R. Caianiello' dell'Università and Gruppo Collegato INFN, Salerno, Italy

³⁰ Dipartimento DISAT del Politecnico and Sezione INFN, Turin, Italy

³¹ Dipartimento di Scienze MIFT, Università di Messina, Messina, Italy

³² Dipartimento Interateneo di Fisica 'M. Merlin' and Sezione INFN, Bari, Italy

- ³³ European Organization for Nuclear Research (CERN), Geneva, Switzerland
- ³⁴ Faculty of Electrical Engineering, Mechanical Engineering and Naval Architecture, University of Split, Split, Croatia
- ³⁵ Faculty of Engineering and Science, Western Norway University of Applied Sciences, Bergen, Norway
- ³⁶ Faculty of Nuclear Sciences and Physical Engineering, Czech Technical University in Prague, Prague, Czech Republic
- ³⁷ Faculty of Physics, Sofia University, Sofia, Bulgaria
- ³⁸ Faculty of Science, P.J. Šafárik University, Košice, Slovak Republic
- ³⁹ Frankfurt Institute for Advanced Studies, Johann Wolfgang Goethe-Universität Frankfurt, Frankfurt, Germany
- ⁴⁰ Fudan University, Shanghai, China
- ⁴¹ Gangneung-Wonju National University, Gangneung, Republic of Korea
- ⁴² Gauhati University, Department of Physics, Guwahati, India
- ⁴³ Helmholtz-Institut für Strahlen- und Kernphysik, Rheinische Friedrich-Wilhelms-Universität Bonn, Bonn, Germany
- ⁴⁴ Helsinki Institute of Physics (HIP), Helsinki, Finland
- ⁴⁵ High Energy Physics Group, Universidad Autónoma de Puebla, Puebla, Mexico
- ⁴⁶ Horia Hulubei National Institute of Physics and Nuclear Engineering, Bucharest, Romania
- ⁴⁷ HUN-REN Wigner Research Centre for Physics, Budapest, Hungary
- ⁴⁸ Indian Institute of Technology Bombay (IIT), Mumbai, India
- ⁴⁹ Indian Institute of Technology Indore, Indore, India
- ⁵⁰ INFN, Laboratori Nazionali di Frascati, Frascati, Italy
- ⁵¹ INFN, Sezione di Bari, Bari, Italy
- ⁵² INFN, Sezione di Bologna, Bologna, Italy
- ⁵³ INFN, Sezione di Cagliari, Cagliari, Italy
- ⁵⁴ INFN, Sezione di Catania, Catania, Italy
- ⁵⁵ INFN, Sezione di Padova, Padova, Italy
- ⁵⁶ INFN, Sezione di Pavia, Pavia, Italy
- ⁵⁷ INFN, Sezione di Torino, Turin, Italy
- ⁵⁸ INFN, Sezione di Trieste, Trieste, Italy
- ⁵⁹ Inha University, Incheon, Republic of Korea
- ⁶⁰ Institute for Gravitational and Subatomic Physics (GRASP), Utrecht University/Nikhef, Utrecht, Netherlands
- ⁶¹ Institute of Experimental Physics, Slovak Academy of Sciences, Košice, Slovak Republic
- ⁶² Institute of Physics, Homi Bhabha National Institute, Bhubaneswar, India
- ⁶³ Institute of Physics of the Czech Academy of Sciences, Prague, Czech Republic
- ⁶⁴ Institute of Space Science (ISS), Bucharest, Romania
- ⁶⁵ Institut für Kernphysik, Johann Wolfgang Goethe-Universität Frankfurt, Frankfurt, Germany
- ⁶⁶ Instituto de Ciencias Nucleares, Universidad Nacional Autónoma de México, Mexico City, Mexico
- ⁶⁷ Instituto de Física, Universidade Federal do Rio Grande do Sul (UFRGS), Porto Alegre, Brazil
- ⁶⁸ Instituto de Física, Universidad Nacional Autónoma de México, Mexico City, Mexico
- ⁶⁹ iThemba LABS, National Research Foundation, Somerset West, South Africa
- ⁷⁰ Jeonbuk National University, Jeonju, Republic of Korea
- ⁷¹ Johann-Wolfgang-Goethe Universität Frankfurt Institut für Informatik, Fachbereich Informatik und Mathematik, Frankfurt, Germany
- ⁷² Korea Institute of Science and Technology Information, Daejeon, Republic of Korea
- ⁷³ KTO Karatay University, Konya, Turkey
- ⁷⁴ Laboratoire de Physique Subatomique et de Cosmologie, Université Grenoble-Alpes, CNRS-IN2P3, Grenoble, France
- ⁷⁵ Lawrence Berkeley National Laboratory, Berkeley, California, United States
- ⁷⁶ Lund University Department of Physics, Division of Particle Physics, Lund, Sweden
- ⁷⁷ Nagasaki Institute of Applied Science, Nagasaki, Japan
- ⁷⁸ Nara Women's University (NWU), Nara, Japan
- ⁷⁹ National and Kapodistrian University of Athens, School of Science, Department of Physics, Athens, Greece
- ⁸⁰ National Centre for Nuclear Research, Warsaw, Poland
- ⁸¹ National Institute of Science Education and Research, Homi Bhabha National Institute, Jatni, India
- ⁸² National Nuclear Research Center, Baku, Azerbaijan
- ⁸³ National Research and Innovation Agency - BRIN, Jakarta, Indonesia

- ⁸⁴ Niels Bohr Institute, University of Copenhagen, Copenhagen, Denmark
⁸⁵ Nikhef, National institute for subatomic physics, Amsterdam, Netherlands
⁸⁶ Nuclear Physics Group, STFC Daresbury Laboratory, Daresbury, United Kingdom
⁸⁷ Nuclear Physics Institute of the Czech Academy of Sciences, Husinec-Řež, Czech Republic
⁸⁸ Oak Ridge National Laboratory, Oak Ridge, Tennessee, United States
⁸⁹ Ohio State University, Columbus, Ohio, United States
⁹⁰ Physics department, Faculty of science, University of Zagreb, Zagreb, Croatia
⁹¹ Physics Department, Panjab University, Chandigarh, India
⁹² Physics Department, University of Jammu, Jammu, India
⁹³ Physics Program and International Institute for Sustainability with Knotted Chiral Meta Matter (SKCM2), Hiroshima University, Hiroshima, Japan
⁹⁴ Physikalisches Institut, Eberhard-Karls-Universität Tübingen, Tübingen, Germany
⁹⁵ Physikalisches Institut, Ruprecht-Karls-Universität Heidelberg, Heidelberg, Germany
⁹⁶ Physik Department, Technische Universität München, Munich, Germany
⁹⁷ Politecnico di Bari and Sezione INFN, Bari, Italy
⁹⁸ Research Division and ExtreMe Matter Institute EMMI, GSI Helmholtzzentrum für Schwerionenforschung GmbH, Darmstadt, Germany
⁹⁹ Saga University, Saga, Japan
¹⁰⁰ Saha Institute of Nuclear Physics, Homi Bhabha National Institute, Kolkata, India
¹⁰¹ School of Physics and Astronomy, University of Birmingham, Birmingham, United Kingdom
¹⁰² Sección Física, Departamento de Ciencias, Pontificia Universidad Católica del Perú, Lima, Peru
¹⁰³ Stefan Meyer Institut für Subatomare Physik (SMI), Vienna, Austria
¹⁰⁴ SUBATECH, IMT Atlantique, Nantes Université, CNRS-IN2P3, Nantes, France
¹⁰⁵ Sungkyunkwan University, Suwon City, Republic of Korea
¹⁰⁶ Suranaree University of Technology, Nakhon Ratchasima, Thailand
¹⁰⁷ Technical University of Košice, Košice, Slovak Republic
¹⁰⁸ The Henryk Niewodniczanski Institute of Nuclear Physics, Polish Academy of Sciences, Cracow, Poland
¹⁰⁹ The University of Texas at Austin, Austin, Texas, United States
¹¹⁰ Universidad Autónoma de Sinaloa, Culiacán, Mexico
¹¹¹ Universidade de São Paulo (USP), São Paulo, Brazil
¹¹² Universidade Estadual de Campinas (UNICAMP), Campinas, Brazil
¹¹³ Universidade Federal do ABC, Santo Andre, Brazil
¹¹⁴ Universitatea Nationala de Stiinta si Tehnologie Politehnica Bucuresti, Bucharest, Romania
¹¹⁵ University of Cape Town, Cape Town, South Africa
¹¹⁶ University of Derby, Derby, United Kingdom
¹¹⁷ University of Houston, Houston, Texas, United States
¹¹⁸ University of Jyväskylä, Jyväskylä, Finland
¹¹⁹ University of Kansas, Lawrence, Kansas, United States
¹²⁰ University of Liverpool, Liverpool, United Kingdom
¹²¹ University of Science and Technology of China, Hefei, China
¹²² University of South-Eastern Norway, Kongsberg, Norway
¹²³ University of Tennessee, Knoxville, Tennessee, United States
¹²⁴ University of the Witwatersrand, Johannesburg, South Africa
¹²⁵ University of Tokyo, Tokyo, Japan
¹²⁶ University of Tsukuba, Tsukuba, Japan
¹²⁷ Universität Münster, Institut für Kernphysik, Münster, Germany
¹²⁸ Université Clermont Auvergne, CNRS/IN2P3, LPC, Clermont-Ferrand, France
¹²⁹ Université de Lyon, CNRS/IN2P3, Institut de Physique des 2 Infinis de Lyon, Lyon, France
¹³⁰ Université de Strasbourg, CNRS, IPHC UMR 7178, F-67000 Strasbourg, France, Strasbourg, France
¹³¹ Université Paris-Saclay, Centre d'Etudes de Saclay (CEA), IRFU, Département de Physique Nucléaire (DPhN), Saclay, France
¹³² Université Paris-Saclay, CNRS/IN2P3, IJCLab, Orsay, France
¹³³ Università degli Studi di Foggia, Foggia, Italy
¹³⁴ Università del Piemonte Orientale, Vercelli, Italy
¹³⁵ Università di Brescia, Brescia, Italy
¹³⁶ Variable Energy Cyclotron Centre, Homi Bhabha National Institute, Kolkata, India

¹³⁷ Warsaw University of Technology, Warsaw, Poland

¹³⁸ Wayne State University, Detroit, Michigan, United States

¹³⁹ Yale University, New Haven, Connecticut, United States

¹⁴⁰ Yonsei University, Seoul, Republic of Korea

¹⁴¹ Zentrum für Technologie und Transfer (ZTT), Worms, Germany

¹⁴² Affiliated with an institute covered by a cooperation agreement with CERN

¹⁴³ Affiliated with an international laboratory covered by a cooperation agreement with CERN.